



Magma recharge in persistently active basaltic–andesite systems and its geohazards implications: the case of Villarrica volcano, Chile

J. A. Cortés¹ · R. Gertisser² · E. S. Calder³

Received: 14 November 2023 / Accepted: 9 April 2024 / Published online: 10 May 2024
© The Author(s) 2024

Abstract

We report whole-rock chemistry, mineral chemistry, and volatile content from Villarrica volcano's major recent paroxysms and background activity. Composition of the volcanic products are basalt to basaltic andesite with whole-rock SiO₂ content between 50 and 56 wt%, and a mineralogy dominated by olivine (Fo_{71–80}), clinopyroxene (Mg# ~ 50) and plagioclase (An_{60–80}). Volatile contents in melt inclusions are up to 1.5 wt% H₂O, 500 ppm CO₂, 1230 ppm sulfur and 580 ppm chlorine. Regardless of the type of activity, there are no substantial variations in whole-rock composition or the volatile content when the activity switches from background activity to a major paroxysm, strongly suggesting that this shift does not just depend on the arrival of new magma in the shallow magmatic system. Geothermobarometry constrains crystallization of the major mineral phases at various depths between 3 and 12.7 km, suggesting that degassing of a volatile-rich recharge magma occurs deeper than 12 km, producing efficient mixing throughout the whole system, and sustaining the lava lake activity in Villarrica's summit crater. The occurrence of a permanent lava lake also suggests that the magma recharge must be close to continuous and therefore sudden changes between background and paroxysmal volcanic activity are likely controlled by relatively small changes in the rate of recharge and/or the volatile release rate in the magmatic system. This has important implications for the understanding of eruption triggers and the forecasting of volcanic eruptions.

Keywords Villarrica volcano · Magma recharge · Persistent degassing · Paroxysmal activity

Introduction

Magma recharge and mixing in long-lived volcanic systems are considered the key processes that can trigger volcanic eruptions (e.g., Sparks et al. 1977; Murphy et al. 1998; Eichelberger and Izbekov 2000; Richer et al. 2004; Morgavi et al. 2017), although not always do these processes drive a volcanic system into an eruption (e.g., Popocatepetl: Manguer et al. 2022; Krafla: Blake and Cortés 2018).

In intermediate and evolved magmatic systems, in which the compositional contrast between a resident magma

and a primitive recharge is substantial, the arrival of new magma (e.g., by dyke injection) usually results in an eruption triggered by the remobilization of a resident crystal mush driven by heat and/or mass transfer (e.g., Richer et al. 2004; Bergantz et al. 2015). In these systems it is usually, although not always (e.g., Ruprecht et al. 2020), relatively straightforward to determine the end-member compositions involved in magma recharge and mixing, to estimate the conditions associated with magma recharge (e.g., relative volumes, pressure/depth and temperature), and to constrain the overall process (Sparks and Marshall 1986; Humphreys et al. 2013), although it has been shown that there is often a cryptic dispersal of mafic-magma-derived components in the more evolved host magma (e.g., Humphreys et al. 2013). In terms of numerical modelling of this process and its overall dynamics, it is generally accepted that mushy, crystal-rich resident magmas (e.g., Cashman et al. 2017; Magee et al. 2018; Lissenberg et al. 2019) can be remobilized, and efficiently mixed with a comparatively crystal-poor recharge magma (Bachmann and Bergantz 2006; Bergantz et al. 2015). This means that the ultimate eruptive behavior of

✉ J. A. Cortés
joaquin.cortes@edgehill.ac.uk

¹ Department of Geography and Geology, Edge Hill University, Ormskirk L39 4QP, UK

² School of Geography, Geology and the Environment, Keele University, Keele ST5 5BG, UK

³ School of GeoSciences, The University of Edinburgh, Grant Institute, The King's Buildings, Hutton Road, Edinburgh EH9 3JW, UK

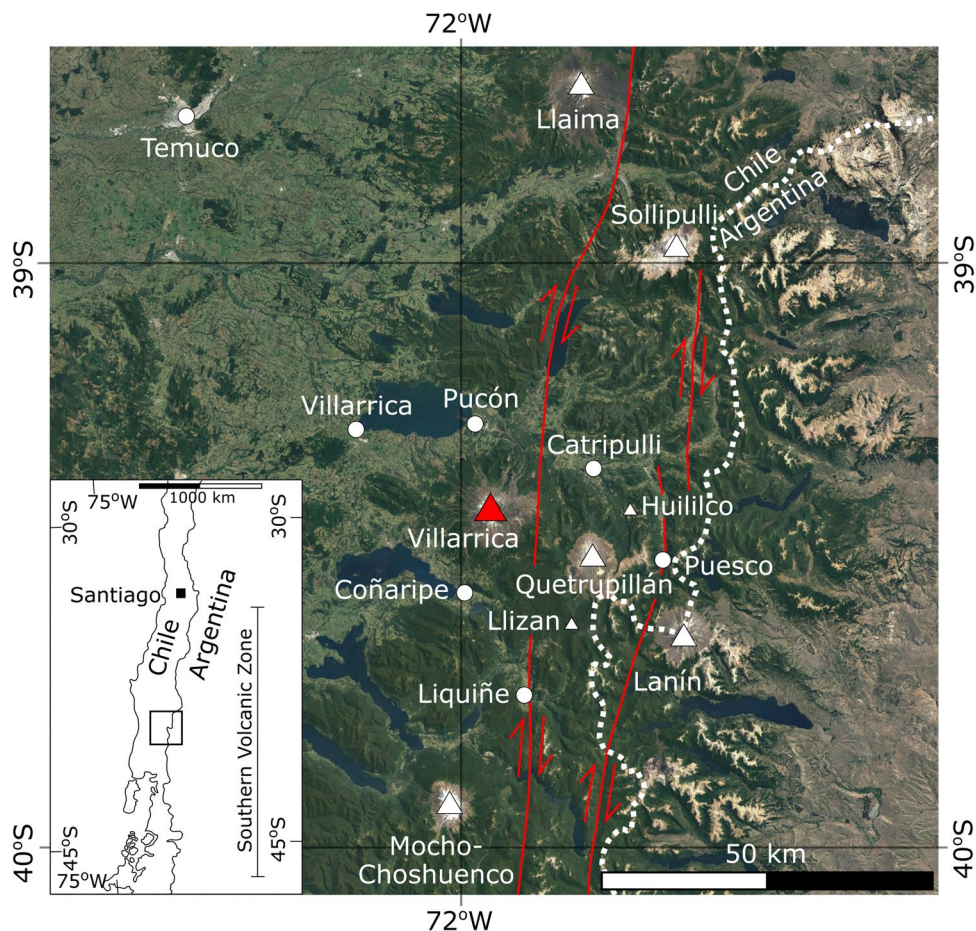
such systems is directly controlled by the volume and frequency of magma recharge, the parameters of which can be measured or estimated by current monitoring techniques.

At the other end of the compositional spectrum lie the primitive magmatic systems (i.e., $\text{SiO}_2 \sim 50\text{--}53$ wt%), in which the differences between a resident magma and a recharge magma are subtle. In these systems, efficient mixing is promoted by similar compositions, thermal conditions and viscosities, and the mechanical stirring from volatile degassing, leading to the generation of a fully hybridized basaltic–andesite magma (e.g., Stromboli: Cortés et al. 2005; Arenal: Streck et al. 2002, 2005), while efficient heat transfer promotes the development and sustainability of a lava lake (e.g., Harris et al. 1999; Moussallam et al. 2016). Another key aspect on these systems is that the arrival of a new mafic recharge in the system does not necessarily culminate in an eruption (Blake and Cortés 2018). Therefore, what dictates the onset of an eruptive episode is the efficiency of the mixing in conjunction with any geometrical constraints imposed by the magma plumbing system (e.g., Cashman et al. 2017; Magee et al. 2018) and its interplay with regional tectonics

(e.g., Cembrano and Lara 2009). As such, a general model of magma recharge and mixing would be complex, without a clear relationship between the arrival of a recharge and an eruptive event.

Here, we are interested on investigating such primitive magmatic systems and specifically, what controls their behavior when new magma arrives in the shallower volcano plumbing. We focus on Villarrica volcano, Chile (39.42°S , 71.93°W ; Fig. 1), a well-known basaltic andesite volcano located in the Southern Volcanic Zone of the Andes (SVZ, Stern 2004), characterized by several relevant historical eruptions (e.g., 1963, 1971, 1984 and 2015) and steady-state activity manifested by a lava lake that has been active since at least 1985 (Calder et al. 2004; Witter et al. 2004; Moussallam et al. 2016). We compare geochemical and textural data between eruptive products of the major historical eruptions and the lavas emplaced during steady state or background activity and examine the link between its eruptive activity and the influence of the local and regional tectonic regime (Cembrano and Lara 2009; Schonwalder-Angel et al. 2018; Simmons et al. 2020a).

Fig. 1 Location of Villarrica volcano (red filled triangle), other volcanic centers in the region (white filled triangles), main settlements (white filled circles) and the two main branches of the Liquiñe-Ofqui Fault zone (red solid lines). The figure shows the Chile-Argentina border with a white dashed line and the inset shows the coverage of the image in relation to the Southern Volcanic Zone of the Andes (see text for more details). Modified from Simmons et al. (2020b); satellite image from Google Earth



Geological background

Basaltic-andesite volcanism in the SVZ

Andean magmatism is a direct consequence of slab dehydration and partial melting of the overlying mantle wedge (López-Escobar et al. 1977; Thorpe 1984). Depending on the crustal thickness, variable degrees of continental crustal contamination may occur (Davidson et al. 1990, 1991; Wörner et al. 1994). In the SVZ, where the crust is relatively thin (~35 km; Cembrano and Lara 2009) and composed predominantly of post-Cretaceous intermediate volcanic rocks, a crustal signature is negligible or difficult to recognize (e.g., Thorpe 1984). Magma residence times at the nearby Puyehue-Cordón Caulle complex (Sigmarsson et al. 2002; Jicha et al. 2007) and Llaima volcano (Reubi et al. 2011) are relatively short (< 1000 yr) as calculated by U–Th–Ra disequilibria in mineral separates, limiting the timescales over which crustal contamination can occur.

More evolved magma compositions and longer residence times may be a function of the regional stress regime (Cembrano and Lara 2009; Schonwalder-Angel et al. 2018; Simmons et al. 2020a). At volcanoes in the compressive tectonic regime of the northern SVZ, prolonged magma storage has resulted in generally more evolved or differentiated (andesitic to dacitic) magmas. Volcanoes located in the central SVZ section (between 37° S and 41.5° S) are influenced by the interplay of dextral-transpressional tectonics in the volcanic arc, associated with the Liquiñe-Ofqui fault zone and compressional stress imposed by the back arc (Göllner et al. 2021). This interaction generates the geometry and the appropriate kinematics for the development of second-order structures such as tension cracks, shear fractures and volcanic fissures, facilitating relatively unimpeded magma ascent from the source, with relatively little time for magmatic differentiation to occur (Cembrano and Lara 2009). The specific tectonic setting hosts the distinctive high alumina basaltic to basaltic-andesite stratovolcanoes of the region, including 13 centers with historical activity (Petit-Breuilh 2006) and several others with post-glacial (< 12.5 ka) activity (Stern et al. 2007).

Villarrica volcano

With more than 60 eruptions $VEI > 2$ since 1553, Villarrica (Fig. 1) is by far the most active volcano in the SVZ of the Andes (Petit-Breuilh 2006; Global Volcanism Programme 2023). Radiogenic and oxygen isotopic compositions suggest that the magma source for its volcanic products is the subcontinental lithospheric mantle enriched by slab-derived fluids or melts, possibly with a minor

component from the lower crust (Tormey et al. 1991; Sigmarsson et al. 2002). Probabilistic analyses of eruption frequency, developed by Dzierma and Wehrmann (2010) and Wehrmann and Dzierma (2011), indicate a probability of a relevant eruption in the range of 60–95% within the next 20 years. Villarrica's latest activity includes a large violent Strombolian explosion on March 3, 2015, intermittent Strombolian activity between September 2018 and August 2019, and large explosions until February 2021. Since then, pervasive seismic activity including continuous tremor signals and crater incandescence punctuated with mild to moderate Strombolian explosions has kept the volcano at a yellow level alert (Global Volcanism Programme 2023).

The presence of an active lava lake (Moussallam et al. 2016) and persistent degassing (Palma et al. 2009, 2011) are evidence of sustained or nearly continuous recharging of the shallow magma reservoir. Punctuating this behavior are regular paroxysmal eruptions (Barberi et al. 1993), the last of which occurred in February 2015 with little seismic warning (Johnson and Palma 2015; Aiuppa et al. 2017). The event culminated in violent Strombolian fountaining (Valentine and Gregg 2008) that lasted ~3 h, later returning to normal levels of background activity characterized by persistent degassing and reappearance of an active lava lake near the vent of the volcanic edifice. Historical explosive eruptions (VEI 2–3) occurred in 1922, 1948, 1963 and 1971, generating > 10 km high eruption columns, and extensive lava flows. During the 1964 eruption, lahars generated by melting of the summit glaciers, caused loss of lives and infrastructure in the town of Coñaripe (Moreno and Clavero 2006; Petit-Breuilh 2006), highlighting the importance of a better understanding of the factors that control the onset of an eruptive event.

Volcanism at Villarrica has been divided into three main stages (Fig. 2), separated by two major caldera-forming events (Moreno and Clavero 2006). Stage I (> 90–14 ka) involved the construction of a large stratocone, which terminated in the caldera-forming Licán Ignimbrite eruption that deposited ~10 km³ (DRE) of basaltic andesite ignimbrite (Clavero 1996; Moreno and Clavero 2006; Lohmar et al. 2007, 2012). Stage II (14–3.7 ka) involved the construction of a second stratocone on the north-western margin of the first caldera and ended in a smaller caldera-forming eruption associated with a ~3.3–5.0 km³ (DRE) basaltic andesite ignimbrite known as the Pucón Ignimbrite (Clavero 1996; Moreno and Clavero 2006; Silva-Parejas et al. 2010). Both major caldera collapses are inferred to have been triggered by the interaction of magma with external water (Lohmar et al. 2007, 2012). Stage III (< 3.7 ka) represents the construction of the currently active cone, again on the north-western margin of the two previous calderas (Fig. 2), characterized by basaltic andesite lavas and pyroclastic successions of violent

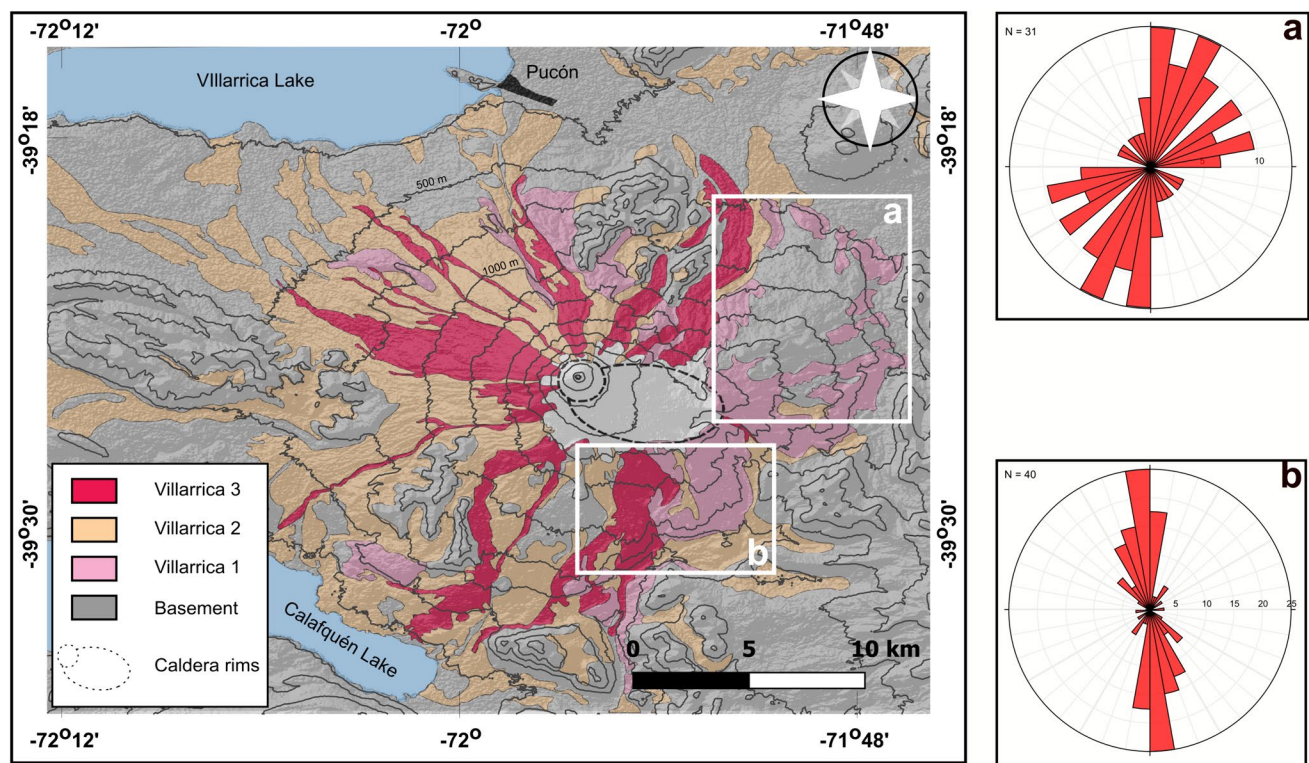


Fig. 2 Simplified geologic map of Villarrica volcano modified from Moreno and Clavero (2006), highlighting the eruptive products of the Villarrica stages 1 (pink), 2 (orange) and 3 (red), and the Holocene calderas associated with the Licán and Pucón ignimbrites (dashed

lines). White boxes in the map indicate the Los Nevados monogenetic field (a) and Chaillupén monogenetic field (b) of Holocene age, in which lineaments were measured. Rose diagrams showing the results of each area are shown to the right of the map

Strombolian to sub-Plinian fallout and surge deposits (Moreno and Clavero 2006; Costantini et al. 2011; Pioli et al. 2015). The volcanic system has also developed two distinctive monogenetic volcanic fields during different stages of activity in the Holocene (Moreno and Clavero 2006), located to the east (Los Nevados) and south of the main volcanic edifice (indicated as “a” and “b” in Fig. 2).

Moreno and Clavero (2006) and Petit-Breuilh (2006) summarized the historical activity at Villarrica since 1553, which has displayed a variety of eruptive styles (e.g., strombolian to violent strombolian with fountaining, lava flows and lahar development) in 1922, 1948, 1964 and 1971, involved significant explosive activity (VEI 2 to 3), and produced extensive lava flows from flank fissures. By contrast, the 1984–1985 eruption (VEI 2) generated only minor lava flows from summit-crater overflow. Current Villarrica products regardless of eruptive style span a narrow compositional range from basalt to basaltic andesite (Hickey-Vargas et al. 1989; Witter et al. 2004; Constantini et al. 2011).

Sample suite and methods

Sample suite

This study focuses on 30 samples that are representative of Villarrica’s different eruptive styles as described in the previous section (Supplementary Table 1). The 1999 and 2000 background activity samples were collected on, or just outside the crater rim during a period when explosive activity in the crater was elevated and the free surface of the lava lake within the crater was relatively high (Ortiz et al. 2003; Calder et al. 2004). The 2004 samples were also collected on the crater rim, but during a time of background degassing, only mild explosive activity, and a withdrawn free lava lake surface (Gurioli et al. 2008). Brief descriptions, sample locations and modal mineralogy of the complete sample set, including samples from the Stage III Chaimilla violent Strombolian fallout deposit (2.6–1.0 ka; Constantini et al. 2011), and from the Holocene Pucón (Lohmar et al. 2007, 2012) and

Licán ignimbrites (Silva-Parejas et al. 2010) are presented in Supplementary Table 1. Additional geochemical data were compiled from previous studies, including those of López-Escobar et al. (1977), Deruelle (1982), Harmon et al. (1984), Hickey-Vargas et al. (1989), Sigmarsson et al. (2002) and Witter et al. (2004).

Methods

Seventy-one lineaments of Holocene monogenetic volcanic structures located to the east (Los Nevados satellite cones; area “a” in Fig. 2) and to the south (Chailupén satellite cones; area “b” in Fig. 2) of Villarrica were measured using Google Earth images (Supplementary Table 3). Fissures were measured directly from the images, while the orientations of the feeder dykes were estimated for each cone following the morphometric approach of Tibaldi (1995). Images were imported and measured in FIJI (Schindelin et al. 2012) equipped with the Strike_Results.ijm plugin (Cortés 2019). Lineament orientations were then imported into Stereonet (Allmendinger et al. 2012; Cardozo and Allmendinger 2013) to generate rose diagrams (Fig. 2a, b).

Whole-rock major and trace-element compositions were determined by X-ray fluorescence spectroscopy at The Open University (UK) and Keele University (UK) using ARL 8420 + dual goniometer wavelength dispersive XRF spectrometers. The estimated reproducibility and accuracy for these analyses, monitored using several in-house rock standards, are better than 1% relative. Loss on ignition (LOI) was determined by heating ~ 1 g of sample material to 900–1050 °C for 1.5–2 h (Supplementary Table 2) and is the total effect of dehydration (loss of weight) and oxidation of ferrous iron (gain of weight). Oxidation often outweighs the effect of dehydration in the analyzed Villarrica samples.

Mineral major element compositions, and major element, S and Cl concentrations in olivine-, clinopyroxene- and plagioclase-hosted melt inclusions and groundmass glasses from scoria from the 1999–2004 period and the 1971 eruption were determined using a CAMECA SX100 electron microprobe at The Open University (UK) with internal PAP correction (Pouchou and Pichoir 1991). Major element glass analyses were obtained using a 20 kV accelerating voltage, 10 nA beam current, a defocused beam (10 µm diameter) and peak counting times per element between 10 and 30 s chosen to minimize the total counting times per analysis. Concentrations of S and Cl were obtained using a 20 kV accelerating voltage, 30 nA beam current, a defocused beam (10–20 µm diameter) and extended peak counting times.

Water and CO₂ concentrations in melt inclusions were analyzed in five olivine-hosted inclusions from the 1971 tephra

and in one clinopyroxene-hosted from the background using a Thermo Nicolet Nexus FTIR spectrometer coupled with a Continuum IR microscope at The Open University. For all spectra, a standard EverGlo mid-infrared source optics, Ge-on-KBr beamsplitter and a liquid nitrogen-cooled MCT-A* detector (11,700–750 cm⁻¹) were used. Concentrations of H₂O were calculated from the height of the total water (i.e., molecular H₂O + OH⁻) peak at 3550 cm⁻¹, using the Beer–Lambert law: $H_2O \text{ (wt\%)} = 10 \times (MA/\rho de)$, where M is the molecular weight of H₂O (18.02), A is the height of the absorption peak, ρ is the sample density (g/l), d is the sample thickness (cm) and ϵ is the molar absorption coefficient (l mol⁻¹ cm⁻¹). Sample thicknesses ($\pm 3 \mu\text{m}$) were measured using a Mitutoyo Digimatic Indicator. The calculated glass density (2844 kg/m³) is that for the average Villarrica melt inclusion composition measured, assuming a nonlinear temperature dependence of melt volume. For all calculations, a molar absorption coefficient at 3550 cm⁻¹ of 63 l/mol-cm was assumed.

Fifty-nine melt inclusions hosted in olivine crystals separated from samples from the major eruptive events (1971, 1984 and 2015 eruptions) and from the background activity were measured using the CAMECA ims 4f ion probe (SIMS) at The University of Edinburgh. The instrument is equipped with a Cs microbeam ion source, a He cryo-pump, liquid nitrogen cold trap, and a sample airlock than can hold, pre-pump at working pressures of ~ 3e⁻⁶ Pa and bake eight samples prior to analysis. Individual crystals were first mounted in EpoxiCure resin to prevent beam damage and a high background, and then the epoxy blocks were gold-coated prior deploying in the instrument for analysis.

The modal mineralogy and petrography of selected Villarrica samples (Supplementary Table 1) were determined using a combination of optical petrography and high-resolution back-scattered electron (BSE) images taken on a Hitachi S–4000 Scanning Electron Microscope (SEM). Crystal size distributions (hereafter CSD; Cashman and Marsh 1988; Marsh 1988, 1998; Higgins 2006) of plagioclase was determined using BSE images of representative samples of the different eruptive products (Supplementary Table 1). Images were imported into FIJI (Schindelin et al. 2012), in which best-fit ellipses were applied to determine long and short axes of the different crystals; a minimum of 200 measurements were performed for each mineral phase to have a representative sample of each CSD (Mock and Jerram 2005; Morgan and Jerram 2006). Mean crystal-aspects’ ratios were determined using the CSDSlice methodology of Morgan and Jerram (2006). The fabric was considered massive (i.e., with no foliation) and measurements were not corrected for crystal roundness. Resulting data were exported using the CSD output plugin into CSDCorrections 1.4 (Higgins 2006) to calculate the CSD distribution of each mineral phase. The total slide area, volumetric phase abundance and vesicularity of the samples were determined using FIJI’s built in features.

Results

Tectonic constrains inferred from monogenetic cone lineaments

A main, N-S prevalent orientation was found in the Chaillupén south monogenetic field (40 measurements), while two prevalent orientations, N-S and NE-SW were found in the Los Nevados, east monogenetic field (31 measurements). The measures are consistent with the orientation of the main trace of the LOFZ and the proposed orientation for the maximum compressive stress associated with the dextral transpression of the structure (Göllner et al. 2021; Simmons et al. 2020a) but parallel to the orientation of the fissures that opened in the main edifice during the 1971 eruption (Castruccio and Contreras 2016).

Whole-rock major and trace element geochemistry

The eruptive products of Villarrica volcano range from calc-alkaline basalt to basaltic andesite (50–56 wt% SiO_2 ; Fig. 3, Supplementary Table 2). Juvenile clasts from the Licán and Pucón ignimbrites comprise the more evolved sample cluster (at SiO_2 contents of 54–57 wt%). Subtle major element variations can be observed between the most mafic and more evolved whole-rock compositions (Fig. 4). FeO^* , MgO , and CaO abundances show an overall decrease with increasing SiO_2 , while Na_2O and K_2O contents increase. TiO_2 and P_2O_5 values remain relatively constant over the Villarrica SiO_2 range, whereas Al_2O_3 shows a peaked trend with increasing values up to 53 wt% SiO_2

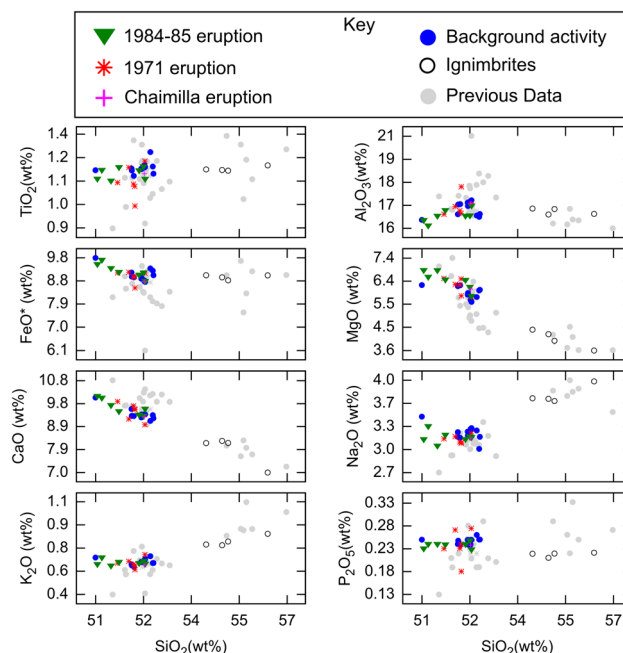


Fig. 4 Major element-variation diagrams in (wt%) vs SiO_2 (wt%) for Villarrica whole-rock samples. All analyses are normalized to 100 wt% on a volatile free basis. Symbols and source of the data as in Fig. 3

and decreasing Al_2O_3 concentrations toward the most evolved basaltic andesites. Similar systematic variations are observed in the trace element concentrations (Fig. 5). Abundances of LILE such as Rb and Ba, increase systematically with increasing SiO_2 , the behavior of Sr resembles that of Al_2O_3 , with a slight increase

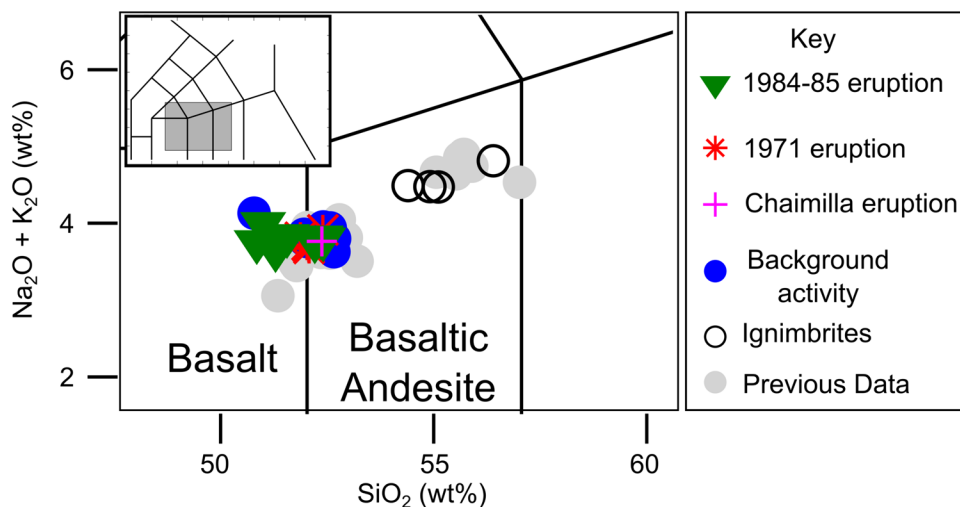


Fig. 3 Total alkali versus SiO_2 classification diagram (Le Maitre et al. 2002) for whole-rock analyses of Villarrica products, showing a clear bimodal distribution with no intermediate compositions between historical lavas (1984–1985 products, green solid triangles; 1971 products, red starts) scoriae (Chaimilla deposits, magenta cross;

background crater activity, blue solid circles), and the Holocene ignimbrites, open circles. The figure also shows previously published analyses as solid gray circles from López-Escobar et al. (1977), Deruelle (1982), Hickey-Vargas et al. (1989), Tormey et al. (1991), and Witter et al. (2004)

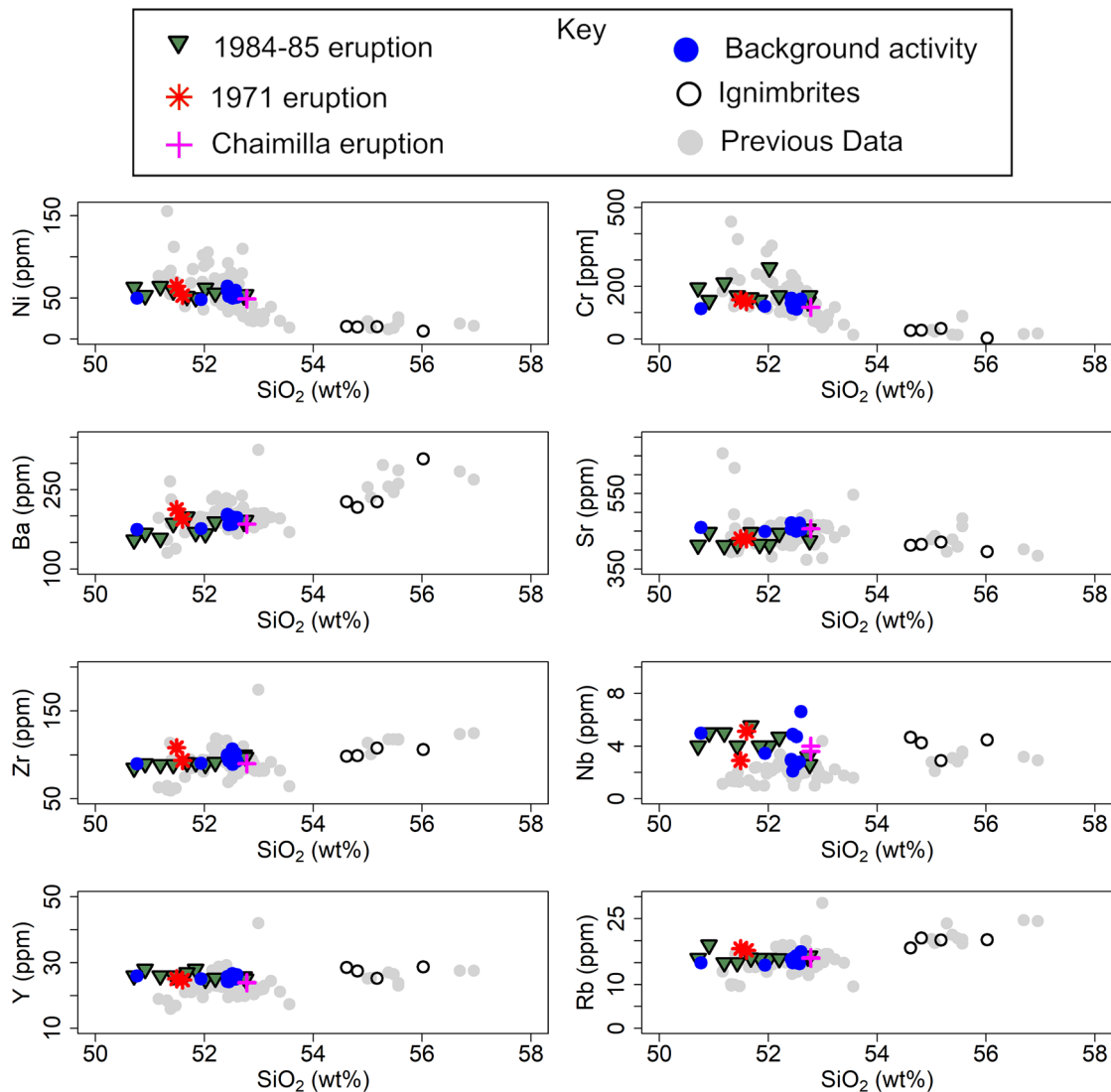


Fig. 5 Selected trace element (ppm) variation diagrams vs SiO_2 (wt%). Symbols and source of the data as in Fig. 3

in the mafic rock types with less than 53 wt% SiO_2 and decreasing abundances in more SiO_2 -rich compositions. The high field strength elements (HFSE), such as Zr, Nb behave as incompatible elements throughout the entire Villarrica suite. Among the transition metals, Ni and Cr loosely correlate negatively with SiO_2 . Rb/Zr ratio shows little variation (between 0.14 and 0.22) across all samples and eruptive styles, while the ratio Ni/Zr varies between 0.2 and 0.7 averaging ~ 0.6 for all the products except for the ignimbrites (Fig. 6).

Petrography and mineral chemistry

Texturally, the Villarrica eruptive products range from porphyritic (15–20% phenocrysts) to less porphyritic flow textures (10% of phenocrysts) and are variably vesicular (from 5% in a dense, glassy fragment from the 1984 ice-chilled

lava, to more than 56% in a cauliflower bomb from the Pucón Ignimbrite and reticulites from the background activity).

The main phenocrysts (Supplementary Table 1) are euhedral to subhedral and zoned plagioclase, subhedral to anhedral clinopyroxene, euhedral to subhedral olivine, and a subhedral oxide phase. The groundmass consists of highly vesicular glass (for recent tephra, e.g., samples VILL-99-6 and VILL-00-1) or it is highly crystalline and trachytoid, characterized by the occurrence of microlites of plagioclase, olivine, clinopyroxene and oxides (for most of the historical lava samples, e.g., samples VILL-84-1 and VILL-99-1).

Olivine occurs as a conspicuous phenocryst phase in most of the lava flow samples while it is less common in the samples representing background activity. These phenocrysts are euhedral to subhedral, often with the presence of resorbed rims. For all samples (recent, historical, and Holocene eruptions),

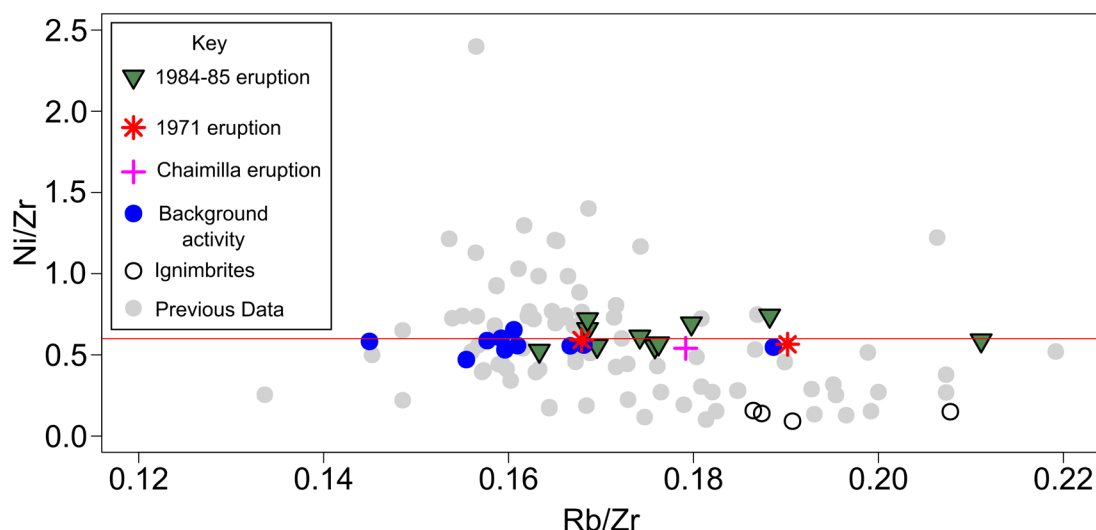


Fig. 6 Rb/Zr versus Ni/Zr diagram of the studied samples and samples from the literature. Symbols and source of the data as in Fig. 3

olivine ranges from Fo₆₉ to Fo₈₆ with an average of Fo₇₆ mol% (Figs. 7a–d, 8a; Supplementary Table 4a).

Small amounts of clinopyroxene occur as euhedral and subhedral, typically unzoned phenocrysts, mainly detected in the background activity scoria (e.g., VILL-99-3, VILL-99-6, VILL-99-7, and VILL-99-10). Representative core-mineral chemistry is reported in Fig. 8b and Supplementary Table 4b. The speciation of iron in clinopyroxene was estimated using charge balance following the approach of Cameron and Papike (1981), while the intrinsic oxygen fugacity was estimated using the relation proposed by Cortés et al. (2006) based on such speciation. Clinopyroxene phenocrysts are mostly confined to the augite field in the pyroxene quadrilateral (Morimoto 1988; Fig. 8a), with two analyses (from sample VILL-99-10) being diopside.

For plagioclase, irrespective of whether the analyses were performed in either core or rim of the crystals, two chemically and texturally distinct populations of phenocrysts are observed in the 1984 samples (Fig. 9). The first population is composed of subhedral, slightly reversely zoned phenocrysts of bytownitic compositions (An_{77–86}), sometimes with ferromagnesian mineral inclusions and melt inclusions that are all indicative of disequilibrium textures. The other population is formed by euhedral to subhedral phenocrysts, which lack both inclusions and zoning, and analyses close to labradoritic compositions (An_{60–69}).

Plagioclase phenocrysts from samples from the 1971 eruption and the Pucón ignimbrite have similar labradoritic compositions (An_{58–68}) and are also texturally similar to

those found in the 1984 lava. Tephra from the background activity has phenocrysts with core compositions showing both bytownitic and labradoritic compositions, while the rims, regardless the core composition are close to a labradoritic composition, similar to plagioclases found in the 1971 lava samples (Supplementary Table 4c).

Oxide phenocrysts are euhedral to subhedral with no ilmenite exsolution, consistent with observations by Witter et al. (2004). Oxides in the recent tephra are typically chromian spinel (Cr# ~ 42–62). Following the cation allocation proposed by Sack and Ghiorso (1991), in terms of the molar proportions of end-members, the average oxides found in the samples have a composition of 34% spinel, 30% magnetite, 8% ulvöspinel, and 28% chromite (Supplementary Table 4d).

Plagioclase crystal size distribution

CSDs of plagioclases were measured in samples from the background activity (samples VILL-01-1, VILL-89-25, VILL-41-25), 1971 lava (samples VILL11-02, VILL11-05A) and 1984 lava (sample VILL11-08). Stereological parameters calculated following Morgan and Jerram (2006) are summarized in Supplementary Table 6.

All plagioclase CSDs lie within a distinct band and range from a steep concave-upward slope to a moderately kinked, straight slope (Fig. 10). Each CSD pattern can be divided into two populations defined by size (> 0.5 mm and < 0.1–0.5 mm), representing two different magma batches. Slope values (based on the straight line calculated with a least square fit) vary between −1.1 and −4.7 [mm^{−1}]

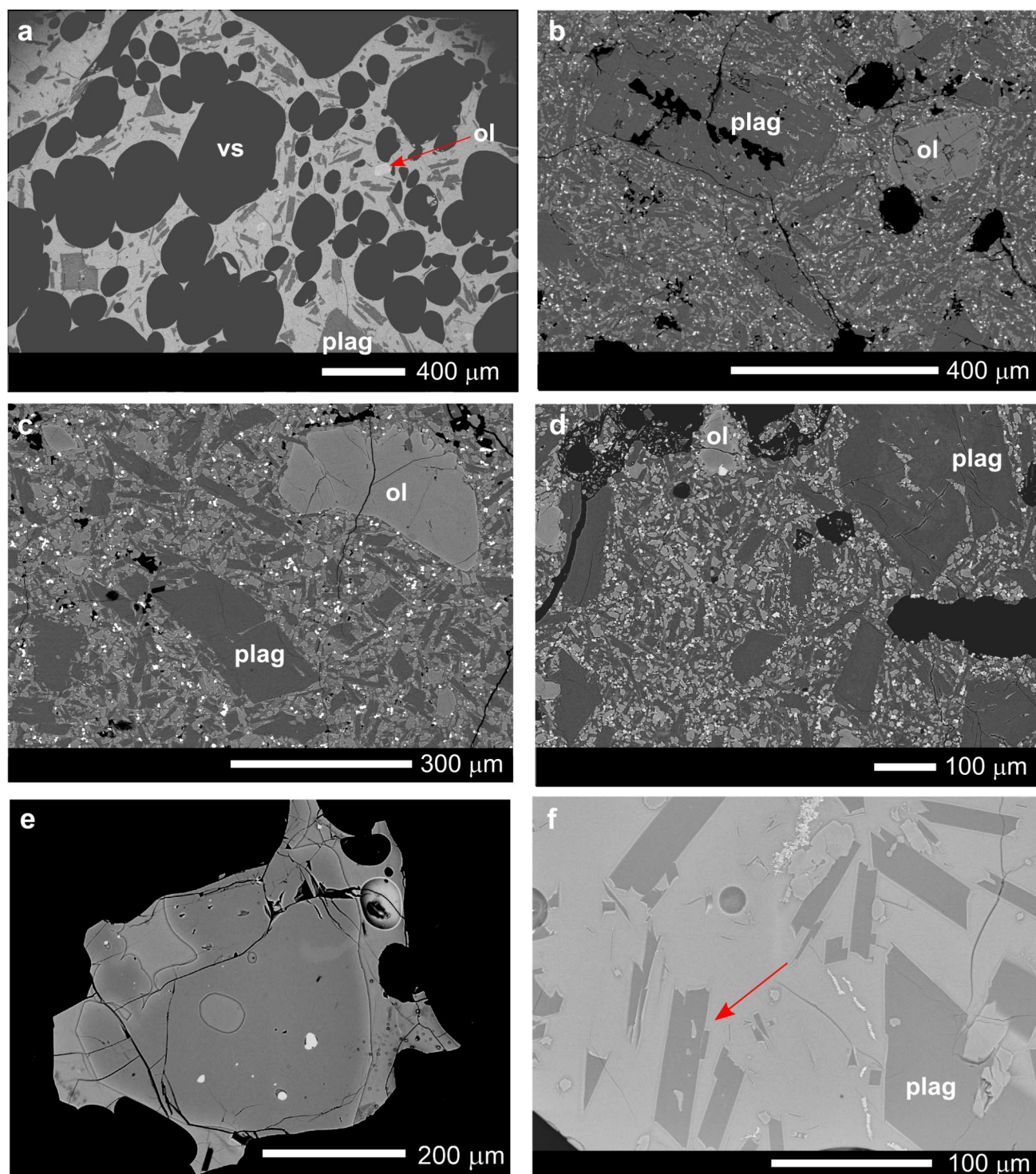


Fig. 7 BSE images of the Villarrica volcanic products. **a** Sample VILL-99-10 (background activity) with plagioclase microlites (plag) and olivines (ol), in a glassy groundmass with 30% of vesicles (vs). **b** 1947 Lava with phenocrysts of plagioclase and olivine in a groundmass of plagioclase, olivine, and oxides. **c** Sample VILL-11-05 (1971 Lava) with phenocrysts of plagioclase and olivine with resorbed rims, in a groundmass of olivine, plagioclase, and oxides. **d** Sample VILL-

99-01 (1984 lava) with mainly plagioclase and minor olivine phenocrysts in an olivine, plagioclase, and oxide groundmass. **e** Olivine phenocryst from sample VILL-99-9 (background activity), hosting chromian spinel inclusions (bright areas) and a round ~30 μm melt inclusion. **f** Sample VILL-99-10 showing plagioclase microlites in a glass matrix. The red arrow points to melt inclusions hosted in one of the microlites. Graphical scales are provided individually

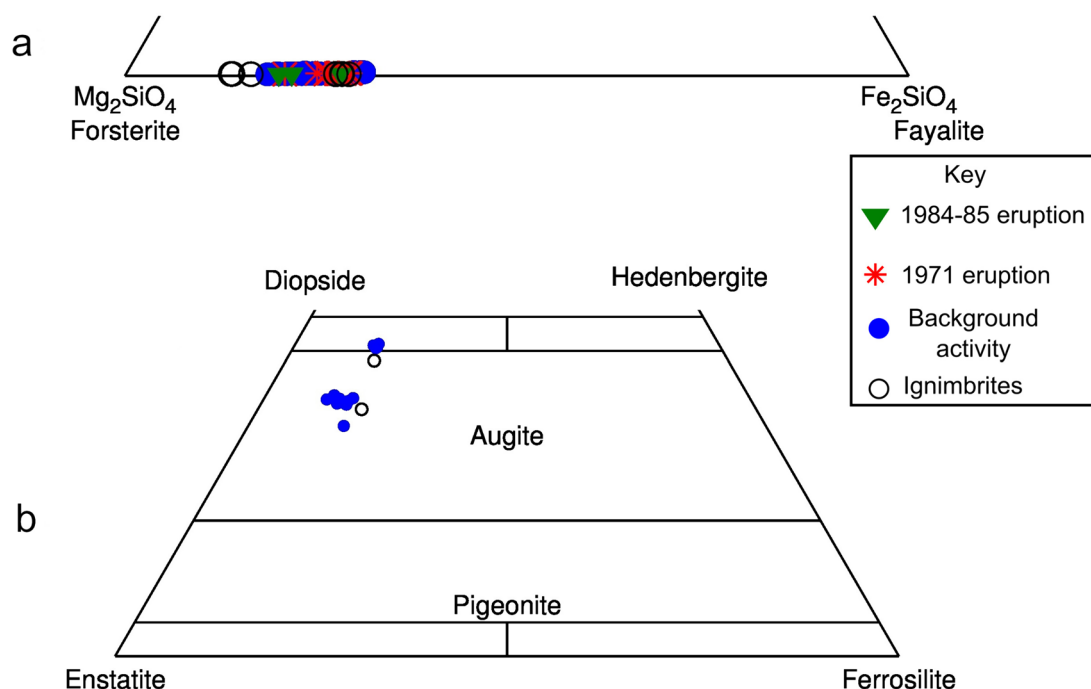


Fig. 8 **a** Olivine compositions based on Fo% from the background activity (blue filled circles), 1971 lava (red asterisks), 1984 lava (solid green triangles) and ignimbrites (open black circles). **b** Pyroxene

quadrilateral classification (Morimoto 1988) with phenocrysts from the background activity (blue filled circles) and the Pucón ignimbrite (open black circles)

for the phenocrysts, and between -16.6 and -55.8 [mm^{-1}] for groundmass populations. In most samples, there is a clear change in the slope of the CSDs (at around 0.5 mm), representing the nucleation and growth of phenocrysts and late-stage groundmass, respectively (Fig. 10).

Based on an average growth rate of $\sim 10^{-8}$ mm/sec, consistent with decompression during ascent (Moschini et al. 2023) residence time can be estimated at ~ 100 days for the phenocrysts and ~ 7 days for the smaller population.

Not considering the smaller population, the CSDs of the plagioclase phenocrysts for both recent products and historical lava flows are similar (Fig. 10).

Major element, S and Cl compositions of melt inclusions and groundmass glass

Melt inclusions in the suite of recent tephra occur in olivine, clinopyroxene and plagioclase phenocrysts. They show variable shapes and sizes, typically consisting of light brown glass and, occasionally, show one or more shrinkage bubbles (Wallace et al. 2015). The melt inclusions trapped in olivine phenocrysts tend to be round, triangular, or irregular in shape, with sizes ranging from < 10 μm to a maximum of ~ 100 μm (Fig. 7e). In rare cases, the melt inclusions display evidence of post-entrapment crystallization (Steele-Macinnis et al. 2011) along the inclusion–host mineral interface or in the form of crystals that extend from the wall into the inclusions. Such melt inclusions were avoided during the analyses. Overall, the studied melt inclusions are typically glassy occasionally containing one, or in rare cases two, small shrinkage bubbles, and appear not to be affected by secondary processes after entrapment occurred, such as

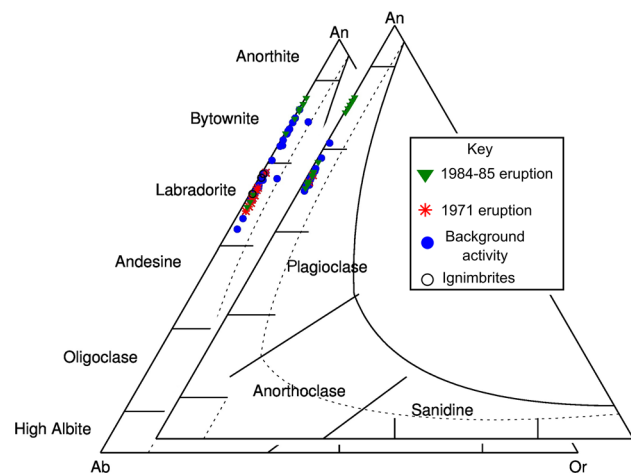


Fig. 9 Plagioclase classification (Deer et al. 2013) from the background activity (blue filled circles), 1971 lava (red asterisks), 1984 lava (solid green triangles), and Holocene ignimbrites (open black circles). The ternary diagram on the left shows core analyses while the one on the right shows rim analyses

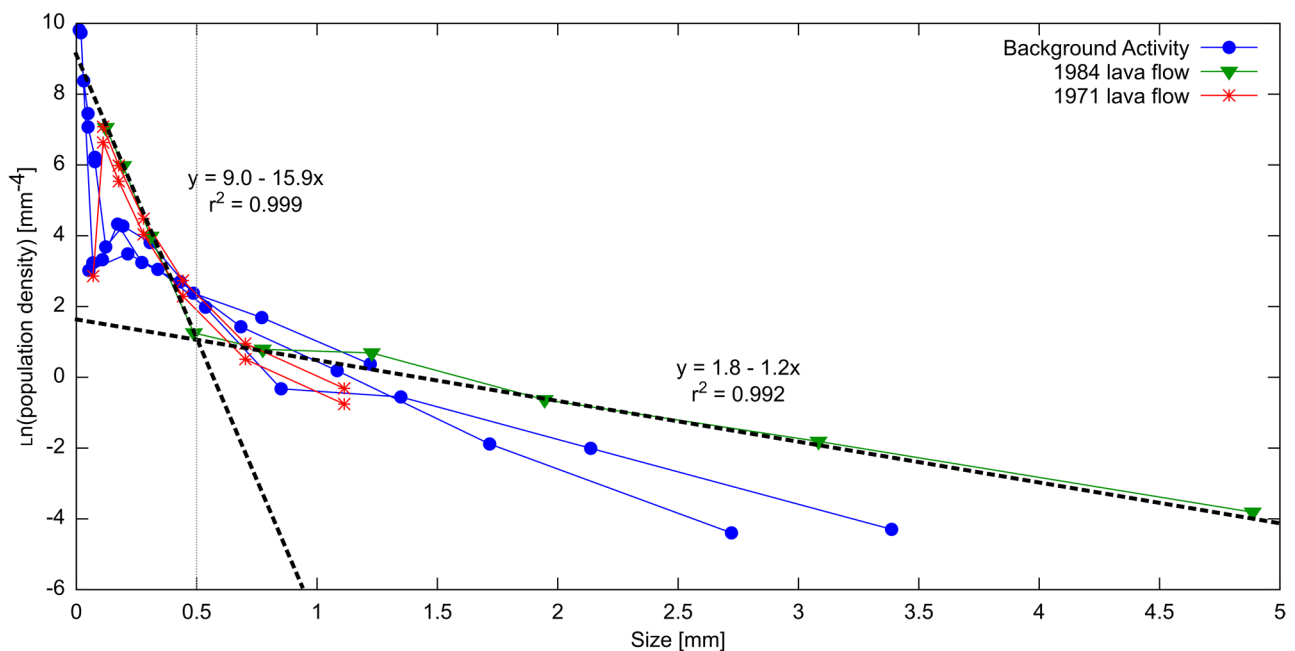


Fig. 10 Natural logarithm of the population density [mm^{-4}] versus size [mm] diagram of the CSDs of plagioclases in samples from the background activity (solid blue circles), 1984 lava (solid green triangles) and 1971 tephra and lava (red asterisks). Dashed lines represent

least square fits to the populations that are smaller and bigger than 0.5 mm for the CSD measured in the 1984 lava sample. Regression line equations and the coefficient of determination (r^2) are also given in the plot

host mineral crystallization along walls or post-entrapment volatile leakage. Melt inclusions are less abundant and smaller ($< 50 \mu\text{m}$) in clinopyroxene, where host mineral crystallization along the inclusion–host mineral interface was frequently observed. Plagioclase-hosted melt inclusions tend to be elongated ($< 100 \mu\text{m}$) and irregular in shape (Fig. 7f). They often appear to be concentrated in the cores of the plagioclase phenocrysts and consist of brown glass, occasionally affected to a minor degree by host mineral crystallization along their boundaries.

A total of 50 melt inclusions in olivine, clinopyroxene and plagioclase and fifty groundmass glasses were analyzed for major elements, sulfur and chlorine (Supplementary Tables 4e, f). Analyses in olivine and clinopyroxene were corrected for post-entrapment crystallization following Putirka (2008) and Simmons et al. (2020a), respectively. After correcting for post-entrapment crystallisation (PEC), reconstructed melt inclusion compositions are basalt to basaltic andesite and show only small variations in major element concentrations (Fig. 11: 52.6–57.9 wt% SiO_2). They are typically more evolved than the corresponding whole-rock compositions, following and extending the trend displayed by the Villarrica whole-rock analyses toward more evolved compositions. The corresponding groundmass glass compositions in the different units vary between 53.6 and 56.1 wt% SiO_2 and are within the same range of values measured in the melt inclusions trapped in the mineral

phases within the same sample when compared on an anhydrous basis (Fig. 11).

The concentration of sulfur in melt inclusions varies considerably from ~ 1230 ppm to values at around and below the microprobe detection limit for sulfur (3σ limit ~ 78 ppm). Only $\sim 25\%$ of the inclusions were found preserving sulfur concentrations in excess of 250 ppm (Supplementary Table 4f, Fig. 12a). Chlorine concentrations in melt inclusions vary from ~ 130 to ~ 600 ppm, although most inclusions cluster around 200 to 300 ppm of chlorine. Our results also show that in general, inclusions with relatively high concentrations of sulfur also preserve relatively high chlorine contents (Fig. 12a). Groundmass glass analyses of scoria yielded sulfur and chlorine concentrations that are significantly lower than those of the melt inclusions, ranging from below the detection limit (see above) to 190 ppm and from ~ 140 to 440 ppm, respectively.

Water and CO_2 concentrations in melt inclusions and groundmass glass

FTIR results (Supplementary Table 5) suggest water contents between 0.3 and 0.8 wt% in the samples from the background activity, consistent with our SIMS results, and a previously published analysis (a single result of 0.29 wt% using SIMS; Witter et al. 2004). Dissolved CO_2 could not be detected using FTIR in any of the analyzed melt

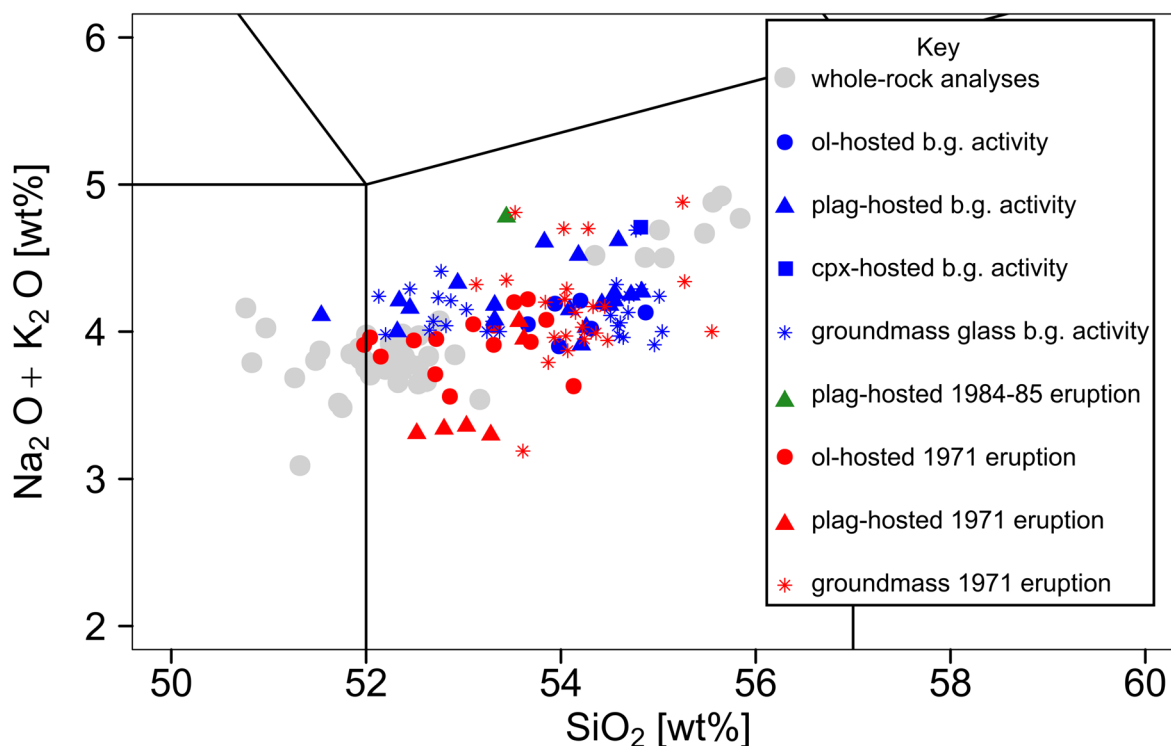


Fig. 11 TAS diagram of melt inclusions hosted in olivine (circles) and plagioclase (triangles), and of groundmass glasses for background tephra (blue crosses) and for the 1971 tephra (red crosses). Colors are red for the 1971 products, green for the 1984 products, and

blue for samples from the background activity. For reference, the diagram also shows in light gray the whole-rock compositions shown in Fig. 3

inclusions (detection limit ~ 100 ppm CO_2). Of the 59 melt inclusions analyzed using SIMS, 15 are from the background activity, 8 from the 1971 tephra, 5 from the 1984 lava and 16 from the 2015 tephra. Regardless the eruption, the melt inclusions contain on average between ~ 100 and 150 ppm of CO_2 and between 0.4 and 0.9 wt% of H_2O , with CO_2 up to 560 ppm and H_2O up to 1.55 wt% (Supplementary Table 5; Fig. 12b). Although in the considered eruptions the range of H_2O values has a wider spread than in the background activity, there is no relationship between the magnitude of the eruptive style and $\text{CO}_2/\text{H}_2\text{O}$ ratios, and high CO_2 content has been measured in some olivine-hosted melt inclusions collected from the background activity (Fig. 12b).

In contrast with similar systems such as Stromboli (Métrich et al. 2001), there is no significant relationship between CO_2 and H_2O content, with melt inclusions containing high CO_2 concentrations and very low- H_2O content (Fig. 12b). As most MIs have a large range of H_2O content at constant and low CO_2 content, i.e., there is no clear degassing path from higher CO_2 concentrations showing a vertical trend at higher H_2O (Fig. 12b), CO_2 degassing is something likely happening deep in the system, and only the shallower pathway of degassing in which H_2O gets reduced at low but constant CO_2 has been recorded in the MIs. There are few

MIs containing relatively high amounts of CO_2 in relation with H_2O content, which could be a consequence of: H^+ diffusion in originally enriched MIs (Gennaro et al. 2019); disequilibrium degassing (Pichavant et al. 2013); diffusive fractionation due to vesiculation and different magma-ascent velocities (Yoshimura 2015); and “ CO_2 fluxing”, due to the flushing of CO_2 through the shallow system (Yoshimura and Nakamura 2013) or magma mixing and convection (Witham 2011).

Magmatic intrinsic conditions

Olivine- and clinopyroxene-melt equilibria

For these calculations, we first estimated the oxidation state of the Villarrica magmas using the speciation of iron in clinopyroxene calculated by charge balance (Cameron and Papike 1981; Cortés et al. 2006). The results (Supplementary Table 3b) constrain the oxidising conditions of the Villarrica magmas at values of 1–2 log units above the fayalite-magnetite-quartz (FMQ) buffer, comparable with previous estimations (e.g., Lohmar et al. 2012) and typical arc magma oxidation values (e.g., Toplis and Carroll 1995).

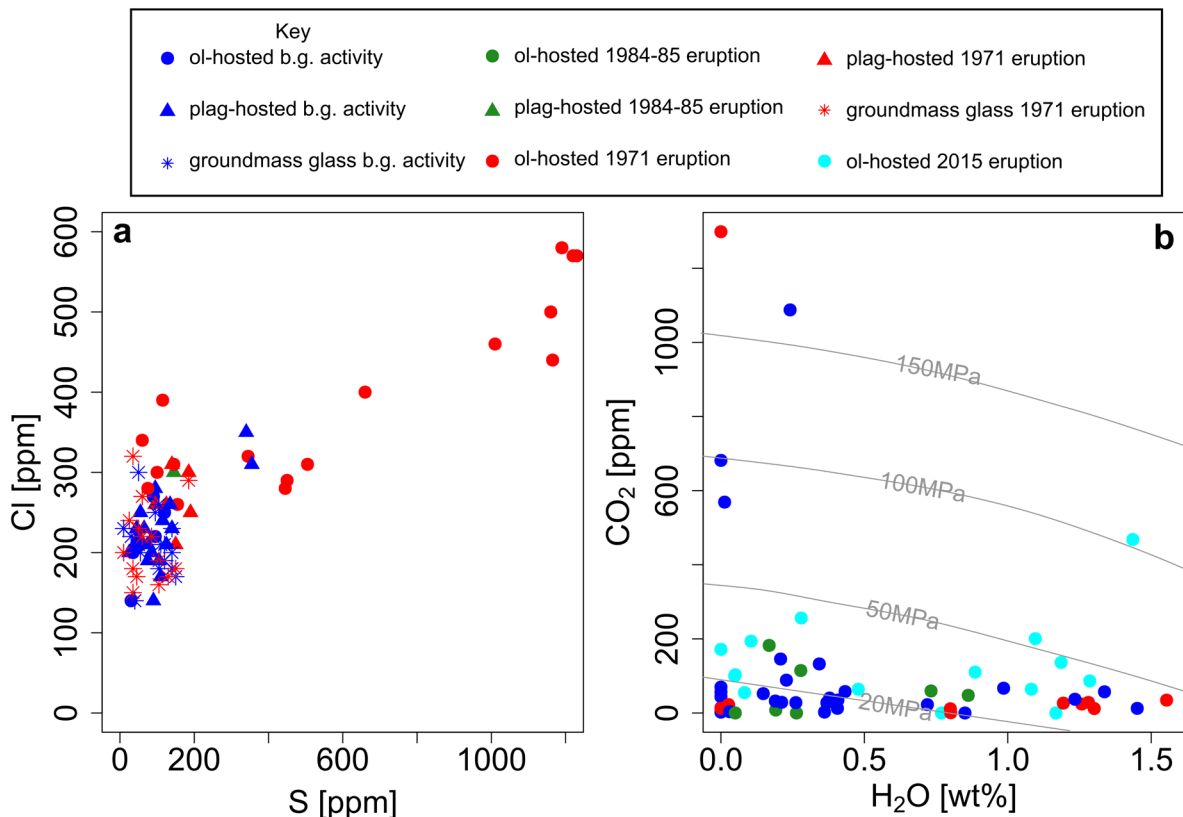


Fig. 12 **a** Plot of chlorine (ppm) vs sulfur (ppm) for melt inclusions hosted in olivine (ol-hosted; solid circle) and plagioclase (plag-hosted; solid triangle) and in groundmass glass (asterisk). Colors are red for the 1971 products, green for the 1984 products, and blue for samples from the background (b.g.) activity. **b** Plot of CO₂ (ppm)

versus H₂O (wt%) for melt inclusions hosted in olivine crystals (solid circles) from samples of the 1971 lava (red), the 1984 lava (green) the 2015 lava (cyan) and the background activity (blue). Gray lines are isobars in MPa at 1300 K (after Papale et al. 2006)

Magmatic temperatures were estimated using olivine-melt equilibrium in melt inclusions and their olivine host following the approach of Putirka (2008). Of all measured pairs (83), only 9 calculations (samples VILL-99-5; VILL-12-12; VILL-12-1-12 and sample VILL-12-13) gave values in which the partition coefficient K_D was $\sim 0.3 \pm 0.05$ between FeO and MgO (Roeder and Emslie 1970), and resulting temperatures of $\sim 1115 \pm 13$ °C (Putirka 2008, Eq. 22), $\sim 1133 \pm 17$ °C (Putirka 2008, Eq. 21), and 1127 °C ± 13 (Beattie 1993).

Only clinopyroxene crystals and melt inclusions found in sample VILL-07 gave values close to equilibrium ($K_D \sim 0.23$ between FeO and MgO, following Putirka 2008). The pairs gave temperatures between 1131 and 1166 °C (Putirka et al. 1996, 2003), consistent with the temperatures from the olivine-melt pairs, and pressures between 90–100 and 250–350 MPa, corresponding to depths of 3–3.5 and 9–12.7 km, respectively, assuming a density of 2800–2900 kg/m³.

Equilibrium between plagioclase and melt

For feldspars, Putirka (2008) introduced a partition coefficient for Na-Ca partitioning between plagioclase and melt. This coefficient is not constant, but temperature dependent ($K_D \sim 0.25$ for $T < 1050$ °C, $K_D \sim 0.1$ otherwise). The criterion suggests that in general, in the Villarrica magmas, plagioclase phenocrysts are far from equilibrium with Villarrica glass compositions. Only a few calculations in samples VILL-99-7 and VILL-99-1 satisfied the equilibrium criterion, yielding temperatures between 1135 and 1194 °C (Putirka 2008, Eq. 23), and water contents clustering at 0.5–0.9 wt% and 1.3–1.8 wt% H₂O (Putirka 2008, Eq. 25a). The values are consistent with some of the measured values using SIMS and FTIR (Supplementary Table 4), in which the measured water content can be considered a minimum value due to possible water loss by diffusion from the melt inclusions.

Discussion

The Villarrica system

To understand the mechanisms that control the Villarrica system, we first evaluate the overall implications of Villarrica's location in relation to the LOFZ (Fig. 1) and its exerted stress field on the volcano (e.g., Simmons et al. 2020a). Our lineament analysis based on the two monogenetic volcanic fields associated with the main volcanic edifice strongly supports that at least since the Holocene, the orientation of the maximum compressive stress at Villarrica is NE-SW, which is consistent with the overall geometry of the LOFZ main branch running N-S, and with its dextral, strike-slip movement associated with regional transpression (Göllner et al. 2021). Our findings are also consistent with the tectonic model proposed at a regional scale by Cembrano and Lara (2009) or locally, at Quetrupillán, by Simmons et al. (2020a). The main implication is a prevalent orientation for the development of tensile stress exerted on the volcanic edifice and the development of fissures, both at the central cone (e.g., 1971 eruption) and at its flanks. As it has been shown at Llaima volcano (Schonwalder-Angel et al. 2018), the tensile stress orientation promotes the unimpeded ascent of magmas through the volcanic system, consistent with the lack of evolved eruptive products at Villarrica (Fig. 3) and their relatively short residence time in the magmatic system.

Following Edmonds et al. (2022), this local tensional regime is also the cause for long term, persistent, pervasive, and efficient deep degassing at Villarrica. Geobarometry suggests that the depth for a second boiling, i.e., degassing associated with crystallization, is at depths of > 12 km (~350 MPa), explaining the lack of CO₂-rich melt inclusions (their actual concentrations are consistent with depths of less than 1 km; Fig. 12b), which would contain ~2500 ppm at depths of ~12 km if they were not degassed (e.g., Pan et al. 1991). Melt inclusions hosted in olivine are consistently degassed, regardless of whether they occur in products from the background activity or the major eruptions. This deep and open-system degassing, in conjunction with the low viscosity of the magmas, is likely to be the main mechanism to produce pervasive and efficient mixing of resident and recharging magma (Moussallam et al. 2016; Risso 2018; Boschetty et al. 2022; Edmonds et al. 2022), consistent with some CO₂-rich/H₂O-poor melt inclusions (Witham 2011). The mechanical effect of bubble nucleation and growth is likely the agent to promote efficient mass and heat transfer within the Villarrica system, as the buoyant bubbles help to entrain the recharge melt into the resident magma (Wiesmaier et al. 2015). The mechanism is also required to sustain the presence of a permanent lava lake at the vent

(Moussallam et al. 2016). The permanent activity of the lava lake and the persistent degassing strongly suggest that the arrival of a volatile-rich recharge is a nearly continuous process in the Villarrica system.

Results from geothermobarometry confirm the presence of two depths in the transcrustal system, where magmas pond and form crystal mush zones located at 9–12.7 km and at around 3–3.5 km, consistent with previous estimations (Morgado et al. 2015; Boschetty et al. 2022). Measurements of plagioclase CSD constrain the timescale for the continuous pervasive mixing between the reservoirs to days/months.

Background activity vs major eruptions

The above results satisfy the dynamics at Villarrica during background activity, i.e., permanent recharge and degassing, pervasive and continuous mixing sustaining the permanent lava lake at the summit, but they do not explain the sudden shift between background activity and major eruptive events. The crystal size distribution of the plagioclase phase and overall, the petrographic textures among similar eruptive products (e.g., tephra from the background activity and from the 1971 eruption) strongly suggest that, compositionally and chemically, there are no differences between products of the background activity and those products from a major eruption. On the other hand, degassing rates measured prior and during the 2015 eruption show a sudden increase in volatile release rates, which has been related to the separate ascent of over-pressured deeply sourced bubbles (Aiuppa et al. 2017; Edmonds et al. 2022). This interpretation is consistent with the low-H₂O and -CO₂ contents we found in melt inclusions from the 2015 eruption (Supplementary Table 4). In the case of this eruption, or other major historic eruptions, a comparatively more volatile-rich and hotter (but compositionally similar) recharge has been invoked as eruption trigger (Pizarro et al. 2019).

While a substantial change in magma recharge might explain the occurrence of major, paroxysmal events, it fails as a mechanism to explain the background activity, which is permanently sustained between major eruptive events, involving persistent open-system degassing and permanent recharge. An additional issue to consider here is that irrespective of eruption style, the eruptive products are always degassed basaltic andesite. As partial melting of the mantle produces basaltic melt, which evolves while ascending through the transcrustal plumbing system, this constant hybrid composition of the eruptive products further supports a model of continuous injection of evolving melts that subsequently mix efficiently by the mechanical action of the exsolved volatiles (Wiesmaier et al. 2015). Monotonous basaltic andesite compositions at Arenal volcano eruptive

products have been explained similarly (e.g., Streck et al. 2002, 2005).

Therefore, unlike it has been shown at Stromboli (Petrone et al. 2022), we propose that the shift between background activity and a major eruption is not due to the sudden arrival of a substantially more voluminous or different recharge, but rather due to a relatively small increase in the mixing rate and/or the volatile exsolution of a crystal-free recharge into the crystal-mush resident system located at depths of ~12–12.7 km. Based on the CSD of the plagioclase phase, such recharge is occurring permanently likely on a timeframe of days to months under the dynamic but unstable equilibrium conditions that sustain the lava lake. Thus, small changes in the recharge dynamics would have dramatic effects on the resulting eruptive style. As modeled by Bergantz et al. (2015), continuous but low-rate magma injection into a resident crystal mush penetrates and spreads through this mush, while high-rate magma injections would fluidise it, which can then be fully transported into the shallower system and eventually evacuating it. A faster injection would also have the effect of the sudden release of volatiles (e.g., Aiuppa et al. 2017), which would also contribute and enhance the evacuation of the shallower magma system.

Our model explains why there are no fundamental changes between the eruptive products from background and paroxysmal activity, and why melt inclusions in both cases contain similar volatile concentrations. It is also supported by the observation that there are several crystal populations in the eruptive products regardless of the type of activity, as reported by Boschetty et al. (2022). Our model also supports the idea that this switch in eruptive activity can be sudden, with little or no warnings (e.g., Stromboli's 2019 paroxysmal activity, Andronico et al. 2021; Petrone et al. 2022), and with similar timescales of the recharge during background activity.

Conclusions

Villarrica is a basaltic andesite volcanic system with shallow and deep reservoirs (~3 km and ~9–12.7 km, respectively), in which the continuous arrival of a volatile-rich recharge followed by its volatile exsolution and degassing, promotes the continuous and pervasive mixing of their resident magmas. The crystal mush in the lower system is continually but slowly mixed between reservoirs by this process, in which the efficient heat transfer is promoted by the mechanical action of the exsolved volatiles sustaining both the shallow system and the lava lake at the surface during background activity. As magma recharge is a continuous process at Villarrica, its arrival into the system is not what triggers major eruptions, but rather, the small changes in the

recharge injection rate and/or degassing rate of the volatiles, which could abruptly mobilize fully the resident crystal mush into the shallow system producing its sudden evacuation switching the eruptive behavior into a paroxysmal event. Because no substantial changes are required in the magma recharge mechanisms, switching activities might occur in the same timeframe of background activity (i.e., days to few months), posing dramatic implications at Villarrica and similar volcanic systems when forecasting paroxysmic eruptions and their associated hazards.

Supplementary Information The online version contains supplementary material available at <https://doi.org/10.1007/s00531-024-02414-w>.

Acknowledgements This work was partly supported by a Royal Society D. Hodgkin fellowship to ESC while at The Open University. John Watson (The Open University, UK) and David Emley (Keele University, UK) are thanked for carrying out the XRF analyses. Andy Tindle and Sarah Sephton (The Open University) are thanked for assistance with the electron microprobe analyses and the FTIR work, respectively. Work with the ion probe was funded by the IMF664/0518 NERC facility grant. Sarah Chisem (Keele University, UK) is acknowledged for drafting a preliminary version of the geologic map and producing some of the petrographic descriptions used in this work. Rebecca Engasser is acknowledged for measuring the CSD in the samples. Additional samples used in this study were provided by Martina Halmer (Bristol University, UK) and Lucia Gurioli (University Blaise Pascal, Clermont Ferrand, France). The authors acknowledge Ivan Petrinovic and Axel Schmitt for their constructive reviews, and Ulrich Riller for editorial handling. We thank Jenni Barclay and Martin Streck for helpful comments on an earlier version of this work.

Author contributions Joaquín Cortés and Eliza Calder conducted fieldwork at Villarrica and collected the samples. Ralf Gertisser analyzed the whole-rock chemistry of the samples, measure the mineral chemistry of the main mineral phases, and measured volatile content using FTIR. Joaquín Cortés complemented the mineral chemistry and measured the volatile content using SIMS. Joaquín Cortés studied the structural controls at Villarrica. All the authors wrote and edited the current version of the manuscript.

Data availability The data are available on request from the corresponding author.

Open Access This article is licensed under a Creative Commons Attribution 4.0 International License, which permits use, sharing, adaptation, distribution and reproduction in any medium or format, as long as you give appropriate credit to the original author(s) and the source, provide a link to the Creative Commons licence, and indicate if changes were made. The images or other third party material in this article are included in the article's Creative Commons licence, unless indicated otherwise in a credit line to the material. If material is not included in the article's Creative Commons licence and your intended use is not permitted by statutory regulation or exceeds the permitted use, you will need to obtain permission directly from the copyright holder. To view a copy of this licence, visit <http://creativecommons.org/licenses/by/4.0/>.

References

- Aiuppa A, Bitello M, Francoforte V, Velazquez G, Bucarey Parra C, Giudice G, Liuzzo M, Moretti R, Moussallam Y, Peters N, Tamburello G, Valderrama OA, Curtis A (2017) A CO₂-gas precursor to the March 2015 Villarrica volcano eruption. *Geochem Geophys Geosyst* 18:2120–2132. <https://doi.org/10.1002/2017GC006892>
- Allmendinger RW, Cardozo N, Fisher D (2012) Structural geology algorithms: Vectors and tensors in structural geology. Cambridge University Press, Cambridge
- Andronico D, Del Bello E, D'Oriano C, Landi P, Pardini F, Scarlato P, de' Michieli Vituri M, Taddeucci J, Cristaldi A, Ciancitto F, Pennacchia F, Ricci T, Valentini F (2021) Uncovering the eruptive patterns of the 2019 double paroxysm eruption crisis of Stromboli volcano. *Nat Commun* 12:4213. <https://doi.org/10.1038/s41467-021-24420-1>
- Bachmann O, Bergantz GW (2006) Gas percolation in upper-crustal silicic crystal mushes as a mechanism for upward heat advection and rejuvenation of near-solidus magma bodies. *J Volcanol Geotherm Res* 149:85–102. <https://doi.org/10.1016/j.jvolgeores.2005.06.002>
- Barberi F, Rosi M, Sodi A (1993) Volcanic Hazard assessment at Stromboli based on review of historical data. *Acta Vulcanol* 3:173–187
- Beattie P (1993) Olivine-melt and orthopyroxene-melt equilibria. *Contrib Miner Petrol* 115:103–111. <https://doi.org/10.1007/BF00712982>
- Bergantz GW, Schleicher JM, Burgisser A (2015) Open-system dynamics and mixing in magma mushes. *Nat Geosci Lett* 8:793–796. <https://doi.org/10.1038/ngeo2534>
- Blake S, Cortés JA (2018) Forecasting deflation, intrusion and eruption at inflating volcanoes. *Earth Planet Sci Lett* 481:246–254. <https://doi.org/10.1016/j.epsl.2017.10.040>
- Boschetti FO, Fergusson DJ, Cortés JA, Morgado E, Ebmeier SK, Morgan DJ, Romero JE, Silva Parejas C (2022) Insights into magma storage beneath a frequently erupting arc volcano (Villarrica, Chile) from unsupervised machine learning analysis of mineral compositions. *Geochem Geophys Geosyst* 23:333. <https://doi.org/10.1029/2022GC010333>
- Calder ES, Harris AJL, Peña P, Pilger E, Flynn LP, Fuentealba G, Moreno H (2004) Combined thermal and seismic analysis of the Villarrica volcano lava lake, Chile. *Revista Geológica De Chile* 31:259–272. <https://doi.org/10.4067/S0716-02082004000200005>
- Cameron M, Papike JJ (1981) Structural and chemical variations in pyroxenes. *Am Miner* 66:1–50
- Cardozo N, Allmendinger RW (2013) Spherical projections with OSX-Stereonet. *Comput Geosci* 51:193–205. <https://doi.org/10.1016/j.cageo.2012.07.021>
- Cashman KV, Marsh BD (1988) Crystal size distribution (CSD) in rocks and the kinetics and dynamics of crystallization. II: Makaopuhi lava lake. *Contrib Miner Petrol* 99:292–305. <https://doi.org/10.1007/BF00375363>
- Cashman KV, Sparks RSJ, Blundy JD (2017) Vertically extensive and unstable magmatic systems: a unified view of igneous processes. *Science* 355:6331. <https://doi.org/10.1126/science.aag3055>
- Castruccio A, Contreras MA (2016) The influence of effusion rate and rheology on lava flow dynamics and morphology: a case of study from the 1971 and 1988–1990 eruptions at Villarrica and Lonquimay volcanoes, Southern Andes, Chile. *J Volcanol Geoth Res* 327:469–483. <https://doi.org/10.1016/j.jvolgeores.2016.09.015>
- Cembrano J, Lara L (2009) The link between volcanism and tectonics in the southern volcanic zone of the Chilean Andes: a review. *Tectonophysics* 471:96–113. <https://doi.org/10.1016/j.tecto.2009.02.038>
- Clavero J (1996) Ignimbritas andesítico-basálticas postglaciales del Volcán Villarrica, Andes del Sur (39°25'S). Dissertation, Universidad de Chile
- Cortés JA, Wilson M, Condliffe E, Francalanci L (2005) The Evolution of the magmatic system of Stromboli Volcano during the Vancori period (26–13.8 ky). *J Volcanol Geotherm Res* 147:1–38. <https://doi.org/10.1016/j.jvolgeores.2005.03.005>
- Cortés JA, Wilson M, Condliffe E, Francalanci L (2006) The occurrence of Forsterite and highly oxidising conditions in basaltic lavas from Stromboli Volcano, Italy. *J Petrol* 47:1345–1373. <https://doi.org/10.1093/petrology/egl012>
- Cortés, JA (2019). Strike converter 1.0 for ImageJ. <https://thehub.org/resources/4539>. Accessed 16 Oct 2023
- Costantini L, Pioli L, Bonadonna C, Clavero J, Longchamp C (2011) A Late Holocene explosive mafic eruption of Villarrica volcano, Southern Andes: the Chaimilla deposit. *J Volcanol Geoth Res* 200:143–158. <https://doi.org/10.1016/j.jvolgeores.2010.12.010>
- Davidson JP, McMillan NJ, Moorbath S, Wörner G, Harmon RS, López-Escobar L (1990) The Nevados de Payachata volcanic region (18°S/69°W, N. Chile) II. Evidence for widespread crustal involvement in Andean Magmatism. *Contrib Miner Petrol* 105:412–432. <https://doi.org/10.1007/BF01073587>
- Davidson JP, Harmon RS, Wörner G (1991) The source of Central Andean Magmas; some considerations. In: Harmon RS, Rapela CW (eds) Andean magmatism and its tectonic setting. GSA Special Paper, p 265. <https://doi.org/10.1130/SPE265>
- Deer WA, Howie RA, Zussman J (2013) An introduction to the rock forming minerals, 3rd edn. The Mineralogical Society, London
- Deruelle B (1982) Petrology of the Plio-Quaternary volcanism of the south-central and meridional Andes. *J Volcanol Geotherm Res* 14:77–124. [https://doi.org/10.1016/0377-0273\(82\)90044-0](https://doi.org/10.1016/0377-0273(82)90044-0)
- Dzierma Y, Wehrmann H (2010) Eruption time series statistically examined: probabilities of future eruptions at Villarrica and Llaimea Volcanoes, Southern Volcanic Zone, Chile. *J Volcanol Geotherm Res* 193:82–92. <https://doi.org/10.1016/j.jvolgeores.2010.03.009>
- Edmonds M, Liu EJ, Cashman KV (2022) Open-vent volcanoes fuelled by depth-integrated magma degassing. *Bull Volcanol* 84:28. <https://doi.org/10.1007/s00445-021-01522-8>
- Eichelberger J, Izbekov P (2000) Eruption of andesite triggered by dyke injection: contrasting cases at Karymsky volcano, Kamchatka and Mt. Katmai, Alaska. *Philos Trans R Soc Lond A* 358:1465–1485. <https://doi.org/10.1098/rsta.2000.0599>
- Gennaro E, Iacono-Marziano G, Paonita A, Rotolo SG, Martel C, Rizzo AL, Pichavant M, Liotta M (2019) Melt inclusions track melt evolution and degassing of Etnean magmas in the last 15 ka. *Lithos* 324–325:716–732. <https://doi.org/10.1016/j.lithos.2018.11.023>
- Global Volcanism Program (2023) <https://volcano.si.edu/volcano.cfm?vn=357120>. Accessed 15 Oct 2023
- Göllner PL, Eisermann JO, Balbis C, Petrinovic IA, Riller U (2021) Kinematic partitioning in the Southern Andes (39°S–46°S) inferred from lineament analysis and reassessment of exhumation rates. *Int J Earth Sci* 110:2385–2398. <https://doi.org/10.1007/s00531-021-02068-y>
- Gurioli L, Harris AJL, Houghton BF, Polacci M, Rippepe M (2008) Textural and geophysical characterization of explosive basaltic activity at Villarrica volcano. *J Geophys Res* 113:B08206. <https://doi.org/10.1029/2007JB005328>
- Harmon RS, Barreiro BA, Moorbath S, Hoefs J, Francis PW, Thorpe RS, Dérulle B, McHugh J, Vigliani JA (1984) Regional O–Sr and Pb-isotopes relationships in late Cenozoic calc-alkaline lavas of the Andean Cordillera. *J Geol Soc Lond* 141:803–822. <https://doi.org/10.1144/gsjgs.141.5.0803>

- Harris AJL, Flynn LP, Rothery DA, Oppenheimer C, Sherman SB (1999) Mass flux measurements at active lava lakes: implications for magma recycling. *J Geophys Res Solid Earth* 104(B4):7117–7136. <https://doi.org/10.1029/98JB02731>
- Hickey-Vargas R, Moreno-Roa H, López-Escobar L, Frey FA (1989) Geochemical variations in Andean basaltic and silicic lavas from the Villarrica-Lanín volcanic chain (39.5° S): an evaluation of source heterogeneity, fractional crystallization and crustal assimilation. *Contrib Miner Petrol* 103:361–386. <https://doi.org/10.1007/BF00402922>
- Higgins MD (2006) Quantitative textural measurements in igneous and metamorphic petrology. Cambridge University Press, Cambridge
- Humphreys MCS, Edmonds M, Plail M, Barclay J, Parkes D, Christopher T (2013) A new method to quantify the real supply of mafic components to a hybrid andesite. *Contrib Miner Petrol* 165:191–215. <https://doi.org/10.1007/s00410-012-0805-x>
- Jicha BR, Singer BS, Beard BL, Johnson CM, Moreno H, Naranjo JA (2007) Rapid magma ascent and generation of ^{230}Th excesses in the lower crust at Puyehue-Cordón Caulle, Southern Volcanic Zone, Chile. *Earth Planet Sci Lett* 255:229–242. <https://doi.org/10.1016/j.epsl.2006.12.017>
- Johnson JB, Palma JL (2015) Lahar infrasound associated with Volcán Villarrica's 3 March 2015 eruption. *Geophys Res Lett* 42:6324–6331. <https://doi.org/10.1002/2015GL065024>
- Le Maitre RW, Streckeis A, Zanettin B, Le Bas MJ, Bonin B, Bateman P (2002) Igneous rocks; a classification and glossary of terms, 2nd edn. Cambridge University Press, Cambridge
- Lissenberg CJ, MacLeod CJ, Bennett EN (2019) Consequences of a crystal mush-dominated magma plumbing system: a mid-ocean ridge perspective. *Philos Trans R Soc A* 377(2139):20180014. <https://doi.org/10.1098/rsta.2018.0014>
- Lohmar S, Robin C, Gourgaud A, Clavero J, Parada MA, Moreno H, Ersoy O, López-Escobar L, Naranjo JA (2007) Evidence of magma-water interaction during the 13,800 years BP explosive cycle of the Licán Ignimbrite, Villarrica volcano (southern Chile). *Revista Geológica De Chile* 34:233–247. <https://doi.org/10.5027/andgeoV34n2-a04>
- Lohmar S, Parada M, Gutiérrez F, Robin C, Gerbe MC (2012) Mineralogical and numerical approaches to establish the pre-eruptive conditions of the mafic Licán Ignimbrite, Villarrica Volcano (Chilean Southern Andes). *J Volcanol Geoth Res* 235–236:55–69. <https://doi.org/10.1016/j.jvolgeores.2012.05.006>
- López-Escobar L, Frey F, Vergara M (1977) Andesites and high alumina basalts from the central-south Chile, High Andes: geochemical evidences bearing on their petrogenesis. *Contrib Miner Petrol* 63:199–228. <https://doi.org/10.1007/BF00375573>
- Magee C, Stevenson CTE, Ebmeier SK, Keir D, Hammond JOS, Gottsmann JH, Whaler KA, Schofield N, Jackson CAL, Petronis MS, O'Driscoll B, Morgan J, Cruden A, Vollgger SA, Dering G, Micklethwaite S, Jackson MD (2018) Magma plumbing systems: a geophysical perspective. *J Petrol* 59:1217–1251. <https://doi.org/10.1093/ptrology/egy064>
- Mangler MF, Petrone CM, Prytulak J (2022) Magma recharge patterns controls eruption styles and magnitudes at Popocatepetl volcano (Mexico). *Geology* 50:366–370. <https://doi.org/10.1130/G49365.1>
- Marsh BD (1988) Crystal size distribution (CSD) in rocks and the kinetics and dynamics of crystallization I. Theory *Contrib Mineral Petrol* 99:277–291. <https://doi.org/10.1007/BF00375363>
- Marsh BD (1998) On the interpretation of crystal size distributions in magmatic systems. *J Petrol* 39:553–600. <https://doi.org/10.1093/ptrology/39.4.553>
- Métrich N, Bertagnini A, Landi P, Rosi M (2001) Crystallization driven by decompression and water loss at Stromboli Volcano (Aeolian Islands, Italy). *J Petrol* 42:1471–1490. <https://doi.org/10.1093/ptrology/42.8.1471>
- Mock A, Jerram DA (2005) Crystal Size Distributions (CSD) in three dimensions: Insights from the 3D reconstruction of a highly porphyritic rhyolite. *J Petrol* 46:1525–1541. <https://doi.org/10.1093/ptrology/egi024>
- Moreno H, Clavero J (2006) Geología del volcán Villarrica, Regiones de la Araucanía y de Los Lagos. Servicio Nacional de Geología y Minería, Carta Geológica de Chile, Serie Geología Básica 98, Santiago, Chile
- Morgado E, Parada MA, Contreras C, Castruccio A, Gutiérrez F, McGee LE (2015) Contrasting records from mantle to surface of Holocene lavas of two nearby arc volcanic complexes: Caburga-Huelmolle small eruptive centers and Villarrica Volcano, Southern Chile. *J Volcanol Geoth Res* 306:1–16. <https://doi.org/10.1016/j.jvolgeores.2015.09.023>
- Morgan DJ, Jerram DA (2006) On estimating crystal shape for crystal size distribution analysis. *J Volcanol Geoth Res* 154:1–7. <https://doi.org/10.1016/j.jvolgeores.2005.09.016>
- Morgavi D, Arienzo I, Montagna I, Perugini D, Dingwell DB (2017) Magma mixing: history and dynamics of an eruption trigger. In: Gottsmann J, Neuberg J, Scheu B (eds) *Advances in volcanology* 123, volcanic unrest from science to society. Springer, Cham, pp 112–137
- Morimoto N (1988) Nomenclature of pyroxenes. *Mineral Mag* 52:535–550. <https://doi.org/10.1180/minmag.1988.052.367.15>
- Moschini P, Mollo S, Pontesilli A, Nazzari M, Petrone CM, Fanara S, Vona A, Gaeta M, Romano C, Scarlato P (2023) A review of plagioclase growth rate and compositional evolutions in mafic alkaline magmas: guidelines for thermometry, hygrometry, and timescales of magma dynamics at Stromboli and Mt. Etna. *Earth Sci Rev* 240:104399. <https://doi.org/10.1016/j.earscirev.2023.104399>
- Moussallam Y, Bani P, Curtis A, Barnie T, Moussallam M, Peters N, Schipper CI, Aiuppa A, Giudice G, Amigo A, Velazquez G, Cardona C (2016) Sustaining persistent lava lakes: observations from high-resolution gas measurements at Villarrica volcano, Chile. *Earth Planet Sci Lett* 454:237–247. <https://doi.org/10.1016/j.epsl.2016.09.012>
- Murphy MD, Sparks RSJ, Barclay J, Carroll MR, Lejeune AM, Brewer TS, Macdonald R, Black S, Young S (1998) The role of magma mixing in triggering the current eruption at the Soufriere Hills volcano, Montserrat, West Indies. *Geophys Res Lett* 25:3433–3436. <https://doi.org/10.1029/98GL00713>
- Ortiz R, Moreno H, García A, Fuentealba G, Astiz M, Peña P, Sánchez N, Tarraga M (2003) Villarrica volcano (Chile): characteristics of the volcanic tremor and forecasting of small explosions by means of a material failure method. *J Volcanol Geoth Res* 128:247–259. [https://doi.org/10.1016/S0377-0273\(03\)00258-0](https://doi.org/10.1016/S0377-0273(03)00258-0)
- Palma JL, Calder ES, Basualto D, Blake S, Rothery D (2009) Correlations between SO_2 flux, seismicity and outgassing activity at the open vent of Villarrica volcano, Chile. *J Geophys Res* 113:B10201. <https://doi.org/10.1029/2008JB005577>
- Palma JL, Blake S, Calder ES (2011) Constraints on the rates of degassing and convection in basaltic open-vent volcanoes. *Geochem Geophys Geosyst* 12:Q11006. <https://doi.org/10.1029/2011GC003715>
- Pan V, Holloway JR, Hervig RL (1991) The pressure and temperature dependence of carbon dioxide solubility in tholeiitic basalt melts. *Geochim Cosmochim Acta* 55:1587–1595. [https://doi.org/10.1016/0016-7037\(91\)90130-W](https://doi.org/10.1016/0016-7037(91)90130-W)
- Papale P, Moretti R, Barbato D (2006) The compositional dependence of the saturation surface of $\text{H}_2\text{O}+\text{CO}_2$ fluids in silicate melts. *Chem Geol* 229:78–95. <https://doi.org/10.1016/j.chemgeo.2006.01.013>

- Petit-Breuilh ME (2006) La Historia Eruptiva de los volcanes Hispanoamericanos (Siglos XVI al XX). Servicio de Publicaciones Exmo, Cabildo Insular de Lanzarote, Huelva
- Petrone CM, Mollo S, Gertisser R, Buret Y, Scarlato P, Del Bello E, Andronico D, Ellis B, Pontesilli A, De Astis G, Giacomoni PP, Coltorti M, Reagan M (2022) Magma recharge and mush rejuvenation drive paroxysmal activity at Stromboli volcano. *Nat Commun* 13:7717. <https://doi.org/10.1038/s41467-022-35405-z>
- Pichavant M, Di Carlo I, Rotolo SG, Scaillet B, Burgisser A, Le Gall N, Martel C (2013) Generation of CO₂-rich melt during basalt magma ascent and degassing. *Contrib Miner Petrol* 166:545–561. <https://doi.org/10.1007/s00410-013-0890-5>
- Pioli L, Scalisi L, Costantini L, Di Muro A, Bonadona C, Clavero J (2015) Explosive style, magma degassing and evolution in the Chaimilla eruption, Villarrica volcano, Southern Andes. *Bull Volcanol* 77:93–107. <https://doi.org/10.1007/s00445-015-0976-1>
- Pizarro C, Parada MA, Contreras C, Morgado E (2019) Cryptic magma recharge associated with the most voluminous 20th century eruptions (1921, 1948 and 1971) at Villarrica volcano. *J Volcanol Geotherm Res* 384:48–63. <https://doi.org/10.1016/j.jvolgeores.2019.07.001>
- Pouchou JL, Pichoir F (1991) Quantitative analysis of homogeneous or stratified microvolumes applying the model 'PAP.' In: Heinrich KJF, Newbury DE (eds) Electron probe quantitation. Plenum Press, New York, pp 31–75. https://doi.org/10.1007/978-1-4899-2617-3_4
- Putirka K (2008) Thermometers and barometers for volcanic systems. *Rev Mineral Geochem* 69:61–120. <https://doi.org/10.2138/rmg.2008.69.3>
- Putirka K, Johnson M, Kinzler RJ, Longhi J, Walker D (1996) Thermobarometry of mafic igneous rocks based on clinopyroxene-liquid equilibria 0–30 kb. *Contrib Miner Petrol* 123:92–108. <https://doi.org/10.1007/s004100050145>
- Putirka K, Ryerson FJ, Mikaelian H (2003) New igneous thermobarometers for mafic and evolved lava compositions, based on clinopyroxene + liquid equilibria. *Am Miner* 88:1542–1554. <https://doi.org/10.2138/am-2003-1017>
- Reubi O, Bourdon B, Dungan MA, Koornneef JM, Sellés D, Langmuir CH, Aciego S (2011) Assimilation of the plutonic roots of the Andean arc controls variations in U-series disequilibria at Volcán Llaima, Chile. *Earth Planet Sci Lett* 303:37–47. <https://doi.org/10.1016/j.epsl.2010.12.018>
- Richer M, Mann CP, Stix J (2004) Mafic magma injection triggers eruption at Ilopango Caldera, El Salvador, Central America. Geological Society of America, Special Paper, p 375
- Risso F (2018) Agitation, mixing, and transfers induced by bubbles. *Annu Rev Fluid Mech* 50:25–48. <https://doi.org/10.1146/annurev-fluid-122316-045003>
- Roeder PL, Emslie RF (1970) Olivine-liquid equilibrium. *Contrib Miner Petrol* 29:275–289. <https://doi.org/10.1007/BF00371276>
- Ruprecht P, Simon AC, Fiege A (2020) The survival of mafic magmatic enclaves and the timing of magma recharge. *Geophys Res Lett* 47:e2020GL087186. <https://doi.org/10.1029/2020GL087186>
- Sack RO, Ghiorso MS (1991) Chromian spinels as petrogenetic indicators: thermodynamic and petrologic applications. *Am Miner* 76:827–847
- Schindelin J, Arganda-Carreras I, Frise E, Kaynig V, Longair M, Pietzsch T, Preibisch S, Rueden C, Saalfeld S, Schmid B, Tinevez JY, White DJ, Hartenstein V, Eliceiri K, Tomancak P, Cardona A (2012) FIJI: an open-source platform for biological-image analysis. *Nat Methods* 9:676–682. <https://doi.org/10.1038/nmeth.2019>
- Schonwalder-Angel D, Cortés JA, Calder ES (2018) The interplay of magmatism and tectonics: an example based on the satellite scoria cones at Llaima volcano, Chile. *J Volcanol Geotherm Res* 367:31–45. <https://doi.org/10.1016/j.jvolgeores.2018.10.020>
- Sigmarsson O, Chmieleff J, Morris J, Lopez-Escobar L (2002) Origin of ²²⁶Ra-²³⁰Th disequilibria in arc lavas from southern Chile and implications for magma transfer time. *Earth Planet Sci Lett* 196:189–196. [https://doi.org/10.1016/S0012-821X\(01\)00611-2](https://doi.org/10.1016/S0012-821X(01)00611-2)
- Silva Parejas S, Druitt TH, Robin C, Moreno H (2010) The Holocene Pucón eruption of Volcán Villarrica, Chile: deposit architecture and eruption chronology. *Bull Volcanol* 72:677–692. <https://doi.org/10.1007/s00445-010-0348-9>
- Simmons IC, Cortés JA, McGarvie D, Calder ES (2020a) Tectonic constraints on a magmatic plumbing system: the Quetrupillán Volcanic Complex (39°30'S, 71°43'W), Southern Andes, Chile. *J Volcanol Geotherm Res* 407:107101. <https://doi.org/10.1016/j.jvolgeores.2020.107101>
- Simmons IC, McGarvie D, Cortés JA, Calder ES, Pavez A (2020b) Holocene volcanism at the Quetrupillán Volcanic Complex (39° 30' S, 71° 43' W), southern Chile. *Volcanica* 3:115–137. <https://doi.org/10.30909/vol.03.01.115137>
- Sparks RSJ, Marshall LA (1986) Thermal and mechanical constraints on mixing between mafic and silicic magmas. *J Volcanol Geotherm Res* 29:99–124. [https://doi.org/10.1016/0377-0273\(86\)90041-7](https://doi.org/10.1016/0377-0273(86)90041-7)
- Sparks RSJ, Sigmundsson H, Wilson L (1977) Magma mixing: a mechanism for triggering acid explosive eruptions. *Nature* 267:315–318. <https://doi.org/10.1038/267315a0>
- Steele-Macinnis M, Esposito R, Bodnar RJ (2011) Thermodynamic model for the effect of post-entrapment crystallization on the H₂O–CO₂ Systematic of vapor-saturated, silicate melt inclusions. *J Petrol* 52:2461–2482. <https://doi.org/10.1093/petrology/egr052>
- Stern CR (2004) Active Andean volcanism: its geologic and tectonic setting. *Rev Geol Chile* 31:161–208. <https://doi.org/10.4067/S0716-02082004000200000>
- Stern CR, Moreno H, López-Escobar L, Clavero JE, Lara LE, Naranjo JA, Parada MA, Skewes MA (2007) Chilean volcanoes. In: Moreno T, Gibbons W (eds) The geology of Chile. The Geological Society, London, pp 147–178
- Streck M, Dungan M, Malavassi E, Reagan MK, Bussy F (2002) The role of basalt replenishment in the generation of basaltic andesites of the ongoing activity at Arenal volcano, Costa Rica: evidence from clinopyroxene and spinel. *Bull Volcanol* 64:316–327. <https://doi.org/10.1007/s00445-002-0209-2>
- Streck MJ, Dungan MA, Bussy F, Malavassi E (2005) Mineral inventory of continuously erupting basaltic andesites at Arenal volcano, Costa Rica: implications for interpreting monotonous, crystal-rich mafic arc stratigraphies. *J Volcanol Geotherm Res* 140:133–155. <https://doi.org/10.1016/j.jvolgeores.2004.07.018>
- Thorpe RS (1984) The tectonic setting of active Andean volcanism. In: Harmon RS, Barreiro BA (eds) Andean magmatism. Chemical and isotopic constraints. Shiva Geology Series, Bristol, pp 4–8
- Tibaldi A (1995) Morphology of pyroclastic cones and tectonics. *J Geophys Res Solid Earth* 100(B12):24521–24535. <https://doi.org/10.1029/95JB02250>
- Toplis MJ, Carroll MR (1995) An experimental study of the influence of oxygen fugacity on Fe–Ti stability, phase relations and mineral-melt equilibria in ferro-basaltic systems. *J Petrol* 36:1137–1170. <https://doi.org/10.1093/petrology/36.5.1137>
- Tormey DR, Hickey-Vargas R, Frey FA, López-Escobar L (1991) Recent lavas from the Andean volcanic front (33° to 42° S); interpretation along-arc compositional features. In: Harmon RS, Rapela CW (eds) Andean magmatism and its tectonic setting, vol 265. Geological Society of America Special Paper, pp 57–77
- Valentine GA, Gregg TKP (2008) Continental basaltic volcanoes—processes and problems. *J Volcanol Geotherm Res* 177:857–873. <https://doi.org/10.1016/j.jvolgeores.2008.01.050>

- Wallace PJ, Kamenetsky VS, Cervantes P (2015) Melt inclusion CO₂ contents, pressures of olivine crystallisation and the problem of shrinkage bubbles. *Am Mineral* 100:787–794. <https://doi.org/10.2138/am-2015-5029>
- Wehrmann H, Dzierma Y (2011) Applicability of statistical eruption analysis to the geological record of Villarrica and Lanín volcanoes, Southern Volcanic Zone, Chile. *J Volcanol Geotherm Res* 200:99–115. <https://doi.org/10.1016/j.jvolgeores.2010.11.009>
- Wiesmaier S, Morgavi D, Renggli CJ, Perugini D, De Campos CP, Hess KU, Ertel-Ingrisch W, Lavallée Y, Dingwell D (2015) Magma mixing enhanced by bubble segregation. *Solid Earth* 6:1007–1023. <https://doi.org/10.5194/se-6-1007-2015>
- Witham F (2011) Conduit convection, magma mixing, and melt inclusion trends at persistently degassing volcanoes. *Earth Planet Sci Lett* 301:345–352. <https://doi.org/10.1016/j.epsl.2010.11.017>
- Witter JB, Kress VC, Delmelle P, Stix J (2004) Volatile degassing, petrology, and magma dynamics of the Villarrica Lava Lake, Southern Chile. *J Volcanol Geotherm Res* 134:303–337. <https://doi.org/10.1016/j.jvolgeores.2004.03.002>
- Wörner G, Moorbath S, Horn S, Entenmann J, Harmon RS, Davidson JP, Lopez-Escobar L (1994) Large and fine scale geochemical variations along the Andean Arc of Northern Chile (17.5–22° S). In: Reutter KJ, Scheuber E, Wigger PJ (eds) *Tectonics of the Southern Central Andes. Structure and evolution of an active continental margin*. Springer, Berlin, pp 77–92. https://doi.org/10.1007/978-3-642-77353-2_5
- Yoshimura S (2015) Diffusive fractionation of H₂O and CO₂ during magma degassing. *Chem Geol* 411:172–181. <https://doi.org/10.1016/j.chemgeo.2015.07.003>
- Yoshimura S, Nakamura M (2013) Flux of volcanic CO₂ emission estimated from melt inclusions and fluid transport modelling. *Earth Planet Sci Lett* 316:497–503. <https://doi.org/10.1016/j.epsl.2012.11.020>